Linköping studies in science and technology
Licentiate Thesis. No. 1698

System Identification of an Engine-load Setup Using Grey-box Model

Neda Nickmehr

Linköping University
INSTITUTE OF TECHNOLOGY

Department of Electrical Engineering
Linköping University, SE-581 83 Linköping, Sweden

Linköping 2015

Linköping studies in science and technology
Licentiate Thesis. No. 1698

This is a Swedish Licentiate's Thesis.

Swedish postgraduate education leads to a Doctor's degree and/or a Licentiate's degree.
A Doctor's degree comprises 240 ECTS credits (4 years of full-time studies).
A Licentiate's degree comprises 120 ECTS credits,
of which at least 60 ECTS credits constitute a Licentiate's thesis.

Neda Nickmehr
neda.nickmehr@liu.se
www.vehicular.isy.liu.se
Division of Vehicular Systems
Department of Electrical Engineering
Linköping University
SE-581 83 Linköping, Sweden

Nickmehr, Neda
System Identification of an Engine-load Setup Using Grey-box Model
(With Applications in Ride Quality and Misfire Detection for Passenger Cars)
ISBN 978-91-7519-165-2
ISSN 0280-7971

Typeset with LaTeX 2_ε
Printed by LiU-Tryck, Linköping, Sweden 2015

To my dearest, Amir

Abstract

With the demand for more comfortable cars and reduced emissions, there is an increasing focus on model-based system engineering. Therefore, developing accurate vehicle models has become significantly important. The powertrain system, which transfers the engine torque to the driving wheels, is one of the most important parts of a vehicle. Having a reliable methodology, for modeling and parameter estimation of a powertrain structure, helps predict different kinds of behaviors such as torsional vibration which is beneficial for a number of applications in automotive industry. Examples of such cases are ride quality evaluation and model-based fault detection.

This thesis uses the knowledge from the system identification field, which introduces the methods of building mathematical models for dynamical systems based on experimental data, to model the torsional vibration of an engine-load setup. It is a subsystem of the vehicular powertrain and the main source of vibration is the engine fluctuating torque. The challenges are handling a more complicated model structure with a greater number of unknown parameters as well as showing the importance of data information for acquiring better identification performance. Since the engine-load setup is modeled physically here, its state-space equations are available and a grey-box modeling approach can be applied in which the well-known prediction error method is used to estimate the unknown physical parameters. Moreover, a structural identifiability analysis is performed which shows that all of the model parameters are identifiable assuming informative input.

Two main aspects are considered to present an appropriate modeling methodology. The first is simplification of the model structure according to frequency range of interest. This is achieved by performing modal shape analysis to obtain how many degrees-of-freedom are necessary at different frequency ranges. The results show that a 7 degrees-of-freedom model can be simplified to a 2 degrees-of-freedom structure and still have the desired performance for a specific application such as misfire detection.

The second aspect concerns using an appropriate data set, which has the required information for estimation of the unknown parameters. By analyzing the simulation data from a known system, it is shown that the parameters of the 2 degrees-of-freedom model can not be estimated accurately using measurements from a normal combustion data set. However, all the parameters except damping coefficient converge to their true values by using a data set which has misfire in the input torque from the engine. A high estimation variance plus flat loss function indicate that the damping coefficient has no significant influence on the model output and consequently can not be estimated correctly using the available measurements. Thus, to increase the accuracy of the results during estimation on real data, the damping coefficient(s) is assumed to be known. Both the 2 and 7 degrees-of-freedom models are validated against a fresh data set and it is shown that the simulated output captures the important parts of the actual system behavior depending on the application of interest.

Populärvetenskaplig Sammanfattning

Med ökad efterfrågan efter mer komfortabla bilar med minskade utsläpp, finns det ett ökat fokus på modellbaserad systemutveckling. Därför har det blivit viktigt att utveckla mer korrekta matematiska modeller. Drivlinan som överför motorns vridmoment till drivhjulen, är en av de viktigaste delarna av ett fordon. Att ha en tillförlitlig metod för att modellera drivlinan och skatta parametrar i modellen kan förutsäga olika typer av beteenden som vibrationer och vridningar vilket är användbart för ett antal tillämpningar, till exempel utvärdering av körkomfort och modellbaserad diagnos.

Denna avhandling använder kunskap inom systemidentifiering, där matematiska modeller av dynamiska system skattas baserat på experimentella data, för att modellera en motortestbänk som är kopplad till en last. Testbänken består av ett delsystem av drivlinan där den viktigaste källan till vibrationer är motorns vridmoment. Utmaningarna här handlar om att skatta parametrarna hos en mer komplicerad modellstruktur med ett större antal okända parametrar samt att visa betydelsen av hur mycket information som finns i träningsdata och hur det påverkar identifieringen. Eftersom drivlinan modelleras fysikaliskt kallas detta för grey-box-modellering där den välkända prediktionsfelsmetoden används för att skatta de okända fysikaliska parametrarna. Dessutom har en strukturell identifierbarhetanalys genomförts som visar att alla modellparametrar kan identifieras förutsatt att insignalerna är tillräckligt informativa.

Här presenteras två viktiga aspekter kring modelleringsmetodik. Den första är förenkling av modellstrukturen beroende på vilket frekvensområde hos vibrationerna som är av intresse. Detta uppnås genom att utföra modalanalys för att se hur många frihetsgrader som krävs för respektive frekvensområde. Resultaten visar att en drivlinemodell med sju frihetsgrader kan förenklas till en modell med två frihetsgrader och fortfarande modellera intressanta fenomen för tillämpningar så som detektion av missständningar.

Den andra delen fokuserar på hur användningen av tillräckligt informativ data hjälper att skatta de okända parametrarna i modellen. Genom att analysera simuleringsdata från ett känt system, visas att parametrarna för modellen med två frihetsgrader inte kan skattas exakt endast med mätningar från normal förbränning. Alla parametrar utom dämpningskoefficienterna konvergerar till deras verkliga värden med hjälp av data från motorn som innehåller missständningar. En stor varians hos skattningen samt en platt förlustfunktion visar att dämpningskoefficienten inte har betydande inflytande på modellen och kan följaktligen inte beräknas korrekt givet de mätningar som är tillgängliga här. Således, för att öka noggrannheten hos skattningarna baserat på verkliga data antas dämpningskoefficienterna vara kända. Båda modellerna med respektive två och sju frihetsgrader har validerats mot en ny datauppsättning och det visas att den simulerade utsignalen fångar de viktiga delarna av den faktiska systembeteende beroende på tillämpning av intresse.

Acknowledgments

It would not have been possible to write this Licentiate's thesis without the help and support of the kind people around me, to only some of whom it is possible to give particular mention here.

Above all, I would like to thank my beloved husband, Amir, for his personal unlimited kindness, support, and great patience at all times. He was always there cheering me up and stood by me through the good times and bad. My family and specially my mom and dad are always thanked for creating this opportunity for me and giving me the support whenever was necessary.

I would like to express my deepest gratitude to my supervisor, Jan Åslund, for his guidance, caring, patience, and providing me with an excellent atmosphere for doing research. Special thanks go to Erik Frisk and Lars Eriksson for helping me with their valuable fresh ideas and for their patience to answer my questions during these years. I must also acknowledge the head of department, Lars Nielsen, for giving me the opportunity to start Ph.D. study at Vehicular Systems Division. He is thanked for all his support and positive energy. Further thanks go to my colleagues at Vehicular Systems for creating the nice and calm working atmosphere. Daniel Jung and my previous roommate, Andreas Myklebust, are acknowledged for interesting discussions. I thank Jan Åslund, Erik Frisk, Lars Eriksson, and Daniel Jung for reading the thesis and giving me valuable comments. In conclusion, I recognize that this research would not have been possible without the financial assistance of CADICS (a Linnaeus research environment for Control, Autonomy, and Decision-making in Complex Systems) and Linköping University.

Last, but not least, I would like to say many thanks to my nice friends, here in Linköping and even outside Sweden, who always have been there for me and made me happy when the progress at work was very slow. Thank you Atena, Samira, Hoda, Maryam (Sonya) for all your kindness.

Contents

Chapter 1

Introduction

"Essentially, all models are wrong, but some are useful."
- George E.P. Box (1919 - 2013)

A system is known as a device or a set of devices to perform a specific task. This description indicates that a system should have at least one input and one output where there is a cause and effect or action and reaction relationship. Two kinds of systems exist with respect to the input and output connection in time: static and dynamic. The dynamic systems have a memory of the states in which they have been. Whereas the static systems only take the current inputs and convert it to the current outputs without concerning previous inputs values. For example, a simple integrator can be considered as a dynamic system. If the input is a positive constant for this integrator, the output is a ramp which increases linearly in time.

Nowadays, computer simulation techniques are used widely to understand the behavior of dynamic systems in a cheap, safe, and structured way. This requires having a reliable mathematical model for the system which can be obtained by performing two steps. First, a suitable theory is required to describe the system and hence to propose a model structure. Further, an appropriate identification method should be applied to estimate the unknown parameters of the presented model. These are the tasks of system identification field in which the mathematical models are constructed by collecting input and output signals from the actual system.

The dynamic system of interest in this thesis is an engine-load setup, as a subsystem of a passenger car powertrain, which is equipped with a four-cylinder four-stroke Internal Combustion (IC) Spark Ignited (SI) engine. The experimental facility is located at the engine laboratory of Vehicular Systems Division in the Department of Electrical Engineering, Linköping University. The

focus is on the torsional vibration modeling of the crankshaft system exposed to the delivered fluctuating torque from the engine and the required load torque representing, for example, aerodynamic and road excitations.

1.1 Research motivation

A vehicular powertrain is a nonlinear dynamic system which transfers the engine torque to the driving wheels through different subsystems such as engine-block, transmission, differential, and drive shaft. Each subsystem consists of various mechanical components. The focus here is modeling of the engine-block torsional vibration which ends up in a crankshaft rotational behavior study. These vibrations are significantly influenced by different kinds of undesired excitations such as road unevenness or a missing combustion, known as misfire. There exist three important applications in automotive engineering where it is needed to investigate these types of torsional vibrations in powertrain systems:

- Interactions between the powertrain and the car body will affect the vehicle ride quality. In other words, the torsional vibrations of the crankshaft, due to the engine fluctuating torque or any other disturbances, are transported to the wheels through driveline components and result in variations of the drive torque, see Rahnejat (2005). Further, suspension system transfers these variations to the vehicle body and hence the passenger comfort is reduced by the generated longitudinal vibrations. This is studied and published in the following paper:

  – N. Nickmehr, J. Åslund, L. Nielsen, and K. Lundahl. On experimental-analytical evaluation of passenger car ride quality subject to engine and road disturbances. In *The* 19*th International Congress on Sound and Vibration (ICSV19)*. Vilnius, Lithuania, 2012.

  Therefore, car manufacturers are interested in precisely modeling and simulating the powertrain dynamics before the physical prototype production and test. This will not only improve and accelerate the procedures of system design and analysis, but it will also help evaluate the powertrain so that the torsional vibrations are in a desirable range according to the criteria reported by International Standard Organization (ISO) for passenger comfort, see Wong (2008).

- Engine misfire detection is an essential part of the On-Board Diagnostics (OBD) regulations where the aim is to reduce exhaust emissions and avoid damage to the catalytic converters. An overview of misfire detection research is given by Mohammadpour et al. (2012). A great majority of misfire detection algorithms are based on looking at the flywheel angular velocity signal since it is severely influenced by the engine torque, see Connolly and Rizzoni (1994); Kiencke (1999); Tinaut et al. (2007). However,

besides misfire excitation, there exist other possible input disturbances such as cold start, auxiliary load variations, and road load changes that can affect the torsional vibrations of crankshaft angular velocity in a similar way. If these excitations take place at the same time, there is a possibility that their corresponding oscillations have destructive impacts on each other. This may hide the angular velocity response to misfire occurrence and consequently cause difficulties in the detection algorithm, see Eriksson et al. (2013). Moreover, if the second misfire happens close to the first one, it can also have a damaging effect on the detection procedure as shown in Ponti (2008). Accordingly, applying a suitable crankshaft model has two crucial advantages. First, it helps decouple the influences of different disturbances on the crankshaft angular velocity quantitatively. This is valuable for robustness analysis of a misfire detection algorithm to study how large disturbances can be handled. Second, it prevents expensive and time-consuming experimental studies in the developing process of a suitable algorithm for misfire detection.

- The third application of powertrain torsional vibration modeling is in Tire Pressure Indicator (TPI) systems. By having a mathematical model for the powertrain system of a passenger car, the disturbances on the wheel speed signal due to the corresponding engine and driveline torsional vibration can be determined. This will help improve the disturbance cancellation algorithm in the indirect tire pressure monitoring system. A master thesis has been done in NIRA Dynamics AB, Linköping, in which the modeling approach given in Nickmehr et al. (2012) was applied for a specific brand of passenger car, see Johansson (2012). The model parameters were unknown and collected from literature in Johansson (2012). However, using an appropriate parameter estimation technique results in a more accurate disturbance modeling and thus improves the TPI system.

1.2 Goal

The goal of this thesis is to develop a reliable time domain identification method to construct and validate an appropriate model for describing crankshaft torsional vibration subject to the engine fluctuating torque. To achieve this goal, here the following sub-problems are considered. The first is to investigate which type of input and output data set is required for parameter estimation of an engine-load grey-box model. The second issue is to study the simplification of model structure according to the specific application and the frequency range of interest.

1.3 Related research

The crankshaft system can be modeled by torsional elastic elements. The actual

system is distributed, however, basic models comprise linear lumped spring-mass-damper systems which can be extended by additional details about the dynamics of various parts, see Couderc et al. (1998); Crowther (2004). A 6 Degrees-Of-Freedom (DOF) lumped parameter crankshaft model was developed by Rabeih (1997) to describe the engine torsional vibration influences on the entire powertrain of a middle-size passenger car. The proposed model was good enough for simulating free, steady, and transient situations. But, no experimental verification was done. Moreover, the system parameters were selected to be typical, for example, for passenger cars and no further details were provided. However, choosing parameters in this way is not sufficient when a more precise model is needed according to the type of application, see Section 1.1. Schagerberg and McKelvey (2003) studied the dynamic properties of the multi-cylinder engine as the main energy source of the powertrain system. The model was validated against measurements collected during engine tests at several load cases. Ponti (2008), used a similar model as Schagerberg and McKelvey (2003), for the engine block, to simulate multiple misfires. The model in Ponti (2008) was accurate enough to detect and isolate different kinds of multiple misfires using the experimental data from an SI engine. However, the focus of Ponti (2008) was on the detection part and the estimation method was only outlined.

1.4 Contributions

Here, a modular engine-load linear mathematical model, similar to the one given by Ponti (2008), is used to describe crankshaft torsional vibration. The first contribution is using the simplified 2 DOF model to produce input and output data set for simulation study. Further, the loss function analysis is performed to show how much the model simulated output is affected by changing the parameters one by one. The second contribution is to implement the Prediction-Error Method (PEM) for parameter estimation of the 2 DOF and 7 DOF model structures where, by using modal shape analysis, it is shown that each of them is applicable in a specific frequency range. The third contribution is devoted to simulate the effects of different kinds of disturbances, such as misfire, on the system response. An interesting result is the importance of the information in the output signal, subject to these disturbances, for a more accurate system identification.

1.5 Thesis outline

The thesis begins with a general description of system identification in Chapter 2. This is followed by explaining the modeling procedure of the engine-load torsional vibration in Chapter 3. These two chapters give a foundation for understanding of the remaining chapters that are devoted to the contributions. Chapter 4 describes the implementation approach of PEM for system identification of the

engine-load 2 DOF and 7 DOF model structures. Further, the applications in which this kind of modeling is required are proposed in Chapter 5. Finally, Chapter 6 includes conclusions and future work.

1.6 Notation

System identification

Notation	Description
A, B, C	Linear system and measurement matrices
d	Number of unknown parameters
e	White noise signal
f_e	Probability density function
$F(\mathtt{m}, Z^N)$	Model fit for model $\mathtt{m}$ and data set Z
g	Impulse response matrix
G, G_c	Discrete and continuous-time system transfer function
h	Noise filter impulse response matrix
H	Noise transfer function
k	Number of outputs
K	Feedback matrix
l	Scalar-valued function
L	Linear stable filter
m	Number of inputs
$\mathtt{m}$	Estimated model
$\mathbb{M}$	Model structure
N	Number of data points
p	Parameter vector
$\bar{P}$	Covariance matrix of the state estimate error
q	Time shift operator in discrete-time
q^*	Differentiation operator in continuous-time
R_1	Process noise covariance
R_2	Measurement noise covariance
R_{12}	Cross covariance between process noise and measurement noise
$\mathbb{S}$	General notation for dynamic system
t	Time
T_s	Sample time
u	Input vector
v	Measurement noise
v^*	General noise signal
$V_N(p, Z^N)$	Loss function for p based on the data set Z^N
w	Process noise
x	State vector
y	Measurement or output vector
z	System response vector
Z	Input and output data set
ϵ	Prediction-error vector
λ	Levenberg-Marquardt regularization parameter
μ	Optimization step length
ϕ	Regression vector
Φ	Regression matrix
ψ	Prediction-error differentiation with respect to model parameters
$\hat{p}$	Estimated parameter vector
$\dot{x}$	Time derivative
$\hat{x}$	Predicted state vector
$\hat{y}_1(t\|p)$	One-step-ahead-prediction
$\hat{y}_s(t\|\mathtt{m})$	Simulated output of estimated model $\mathtt{m}$

Engine-load mechanical model

Notation	Description
A_p	Piston area
$C_i, C_{i,j}$	Viscous damping coefficient
f	Frequency in Hz
$f(\theta_i^*)$	Crank-slider mechanism expression
F_{pres}	Compression pressure force
F_{inert}	Inertia force
J	Rotating mass inertia
$K_{i,j}$	Stiffness coefficient
L	Connecting rod length
$\mathfrak{m}_{\text{eng}}$	Estimated 2 DOF model using simulation data
$\mathfrak{m}_{\text{eng},r}$	Estimated 2 DOF model using real data
$\mathfrak{m}_{\text{eng},7}$	Estimated 7 DOF model using real data
$\mathbb{M}_{\text{eng}}$	2 DOF Model structure
$\mathbb{M}_{\text{eng},7}$	7 DOF Model structure
n_{cyl}	Number of cylinders
n_{ext}	Number of crankshaft revolutions in which one excitation happens
N	Engine velocity in RPM
$P_{\text{cyl},i}$	Absolute pressure inside ith cylinder
P_{crank}	Crankcase pressure
r	Crank radius
$T_{\text{tot},i}$	Total engine fluctuating torque acting on crank-slider mechanism J_i
T_{load}	Braking dynamometer torque
$T_{\text{ind},i}$	Indicated torque for cylinder i
$T_{\text{recip},i}$	Reciprocating torque for cylinder i
θ	Crank angle
θ_i	Angular position of inertia J_i
θ_i^*	ith cylinder crank angle position
$\theta_{\text{TDC},i}$	ith cylinder top dead center crank angle position
λ_i	Model ith eigenvalue
ω_i	Model ith natural frequency in rad/sec

Abbreviations

Abbreviation	Description
DOF	Degrees-of-freedom
FFT	Fast Fourier transform
IC	Internal combustion
ISO	International standard organization
LSE	Least-squares estimate
LTI	Linear time-invariant
NVH	Noise vibration harshness
OBD	On-board diagnostics
ODE	Ordinary differential equations
OE	Output error
PDF	Probability density function
PEM	Prediction-error method
PO	Parametrized observer
RMS	Root mean square
RPM	Revolution per minute
SI	Spark ignited
TDC	Top dead center
TPI	Tire pressure indicator

List of Figures

List of Tables

Chapter 2

System identification

System identification is a science which addresses the problem of constructing mathematical models for dynamic systems using measured input and output data sets from the system. Once sufficient confidence with the models has been achieved, they can be further used for different applications. In this thesis, the goal is to predict the crankshaft torsional vibration behavior for different inputs by applying a suitable model which can be later utilized to optimize the system performance according to the specific requirements.

This chapter covers some fundamental ideas of system identification. The chapter starts with some definitions about dynamical systems and their characteristics, and then it continues with system identification procedure which has the following specific steps, see Ljung (1999):

1. Three basic entities:
   (a) A set of input-output data
   (b) A model structure
   (c) Identification method
2. Model validation
3. If the obtained model is not able to pass the validation test, then it is necessary to go back and revise different steps of the identification procedure.

Two textbooks which are well-known references on the subject of system identification are Ljung (1999); Söderström and Stoica (1988). These include the details of the subject, both for time and frequency domains system identification. *Perspectives on system identification* is an article by Ljung (2010) in which the author has sketched an overview of basic principles and results in this field.

2.1 Dynamical systems

A dynamic system $\mathbb{S}$ is an object that is influenced by a number of controllable input signals $u(t)$ but also process noise or non-controllable input signals $w(t)$. The system is run by these mentioned inputs and produces a number of outputs $z(t)$, see Figure 2.1. The output measurements $y(t)$ can be further exposed by measurement noise $v(t)$ that is due to the sensors accuracy or the positions where these sensors are located. It is worth mentioning that the system response $z(t)$ is affected by process noise $w(t)$ but not measurement noise $v(t)$. Consequently, the measured outputs of the system can be represented mathematically as follows

$$y = \mathbb{S}(u, w, v) \tag{2.1}$$

in which the mapping is from the entire inputs, $-\infty < t < \infty$, to the entire outputs, $-\infty < t < \infty$. This means that in Figure 2.1, $z(t_1)$ could therefore depend on the values of the inputs, $u(t)$ and $w(t)$, at all time points, i.e. past or future. However, for the engine-load system application the system is causal which means that for every time point t_1, the outputs depend only on the input values up to current time, i.e. time points $-\infty < t < t_1$.

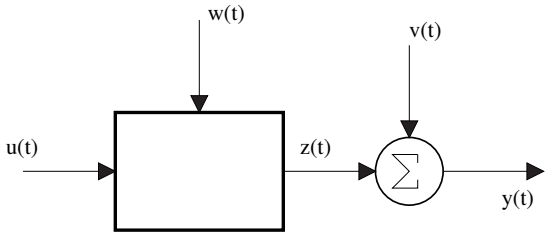

Figure 2.1: *A dynamic system with input, output, process noise, and measurement noise.*

2.1.1 Introduction to vibration systems

Since the application here is torsional vibration modeling of an engine-load system, it is useful to introduce some definitions related to vibration and its classification as well as how vibration studies can be categorized. In this section, the textbook by Liu and Huston (2011) is used as a base to get the whole picture, since it is for automotive application. However, there are some other standard vibration reference books which are suggested for understanding the fundamental concepts, see for example Meirovitch (2010).

What is vibration? Vibration is a phenomenon in which an oscillatory motion occurs for a dynamic system. Figure 2.2 shows different kinds of vibrations that can happen in dynamic systems. Figure 2.2(a) depicts a simple harmonic vibration which is referred to a case where the output of the system can be

described by a single sine or cosine function. Periodic vibration repeats itself in equal time intervals and may possess several frequencies at the same time. In Figure 2.2(b), angular velocity of the damping wheel in an engine-load system is shown as an example of periodic vibration. Transient vibration can be the response of an impulse or a shock acting on a system which is given in Figure 2.2(c). Finally, random vibration, shown in Figure 2.2(d), is a phenomenon in which the output is not deterministic and predictable.

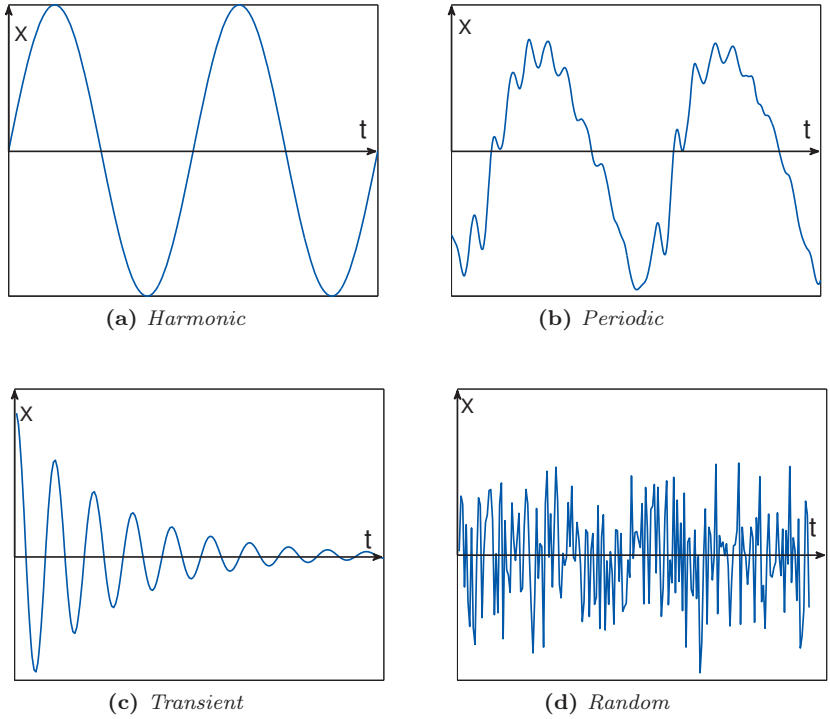

(a) *Harmonic* **(b)** *Periodic*

(c) *Transient* **(d)** *Random*

Figure 2.2: *Different types of vibration in dynamic systems.*

All elastic systems which have masses are capable of vibrations. In this concept, the system inputs $u(t)$ and $w(t)$, mentioned in Section 2.1, can be named excitations. Depending on which of the three factors inputs, outputs, and system properties or parameters that is unknown, there exists four different kinds of studies. First is vibration analysis in which the system characteristics and inputs are known but the outputs behavior is not known. The second kind of investigation, which is known as system design, is done when the inputs and the desired outputs are known and the system should be designed to have the satisfactory performance. The third study is called input evaluation in which the system properties and its outputs are known and the goal is to obtain the

excitations. At last, the fourth case which is also the purpose of this thesis, is system identification where as noted before, the system inputs and outputs are known and the aim is to determine system characteristics. The experimental modal analysis which is famous in vibration field, see Liu and Huston (2011), belongs to this area. However, this method is not used in this thesis and the applied system identification approach is based on the book by Ljung (1999).

2.2 The system identification procedure

In this section, the individual steps of system identification procedure, mentioned in the beginning of this chapter, are described briefly and more inclined towards our specific application.

2.2.1 Model structure

In modeling of a system, the goal is to describe its characteristics appropriate for a specific purpose. It is desirable that the model can, in a sufficient and reliable way, represent the true system. Some how, this step is the most important and simultaneously the most difficult task in the identification procedure. In this thesis, the basic physical laws, mainly Newton's second law, are applied to derive a suitable model for torsional vibrations of an engine-load system subject to the engine fluctuating torque and the braking torque as inputs or excitations. The proposed model has some unknown parameters which are to be estimated. These parameters have physical interpretations, namely inertia, spring, and damping coefficients. This type of modeling, where the structure is known, is called *grey-box* approach according to Ljung (1999).

A note on model structure selection

Modeling is always a trade-off between having a good fit to measurement data from the true system and at the same time having a small number of parameters to estimate. This is called bias-variance conflict, since a good fit means a more flexible model and consequently more unknown parameters to estimate which results in a greater estimation variance and a lower bias. To keep an acceptable compromise between these two important factors for a specific application, it is helpful to involve any valuable knowledge and finding about the system. It might be difficult to end up with the final model structure in one step. For example, it will be shown in Chapter 4 how the engine-load system model can be simplified from a seven-inertias 13th order state-space representation (3.13) in Chapter 3 to a two-inertia 3rd order state-space model for the specific application at hand. This is possible by using the knowledge about which parts of the system to include in the torsional vibration model to acquire a good performance at the desired frequency range. Having this discussion about model structure selection, the next section is devoted to describing classes of models for

Linear Time-Invariant (LTI) systems, since the engine-load torsional vibrations can be fairly good described by a linear and time-invariant model.

Linear model sets and state-space form

The output of a linear system is the weighted sum of the input values at all time instants. As described before, for a causal system only the old values of the inputs are considered, see Glad and Ljung (2000). Moreover, for a time invariant system these weightings are only dependent on the time difference and not the absolute time itself. Accordingly, the output of an LTI model can be represented by its impulse response or in other words by its weighting function

$$y(t) = \int_0^\infty g(\tau)u(t-\tau)d\tau \tag{2.2}$$

where $g(\tau)$ is a $k \times m$ matrix for each τ in which k is the number of outputs and m is the number of inputs. In other words, the element (i, j) of the impulse response $g(\tau)$ is an infinite sequence. In (2.2), a continuous-time representation of the linear system has been given since for many physical applications, the basic relations of the system are provided as differential equations. However, (2.2) can still be used to find the output at desired sampling instants considering that computation of these output values requires numerical solution of a differential equation. Furthermore, by using (2.2) it means that the output of an LTI system can be evaluated once the input signal is known although process and measurement noises are out of our control. If we assume the disturbances are discrete-time and their influence is additive, denoted by $v^*(t)$, the output values at discrete-time instances can be represented as follows

$$y(t) = \int_0^\infty g(\tau)u(t-\tau)d\tau + v^*(t),\ t = 1, 2, \cdots \tag{2.3}$$

where $v^*(t)$ can also be written as a filtered version of white noise $e(t)$, i.e. a sequence of independent (identically distributed) random variables with a specific Probability Density Function (PDF) $f_e(.)$, see Ljung (1999). If the filter impulse response is $h(k)$, the disturbance $v^*(t)$ is described by

$$v^*(t) = \sum_{k=0}^{\infty} h(k)e(t-k). \tag{2.4}$$

Finally, by using the concept of transfer function as well as q^* as the differentiation operator and q as the forward shift operator, the output of an LTI system can be represented by knowing three functions $G_c(q^*)$, $H(q)$, and $f_e(.)$

$$y(t) = G_c(q^*)u(t) + H(q)e(t) \tag{2.5}$$

where c in $G_c(q^*)$ stands for continuous-time. In this way, instead of evaluating infinite sequences $g(\tau)$ and $h(k)$ in (2.2) and (2.4), one needs to obtain a finite

number of parameters that specify the structures of $G_c(q^*)$ and $H(q)$. Therefore, showing the system with its rational transfer functions or state-space formulation, ends up in representation (2.5). Most of the times, not all the coefficients or the parameters of the transfer functions $G_c(q^*)$ and $H(q)$ as well as the PDF $f_e(.)$ are known and they should be estimated which is the task of system identification. For this reason, (2.5) can be written as follows considering the unknown parameters as a vector p, see Ljung (1999),

$$\begin{aligned} y(t) &= G_c(q^*, p)u(t) + H(q, p)e(t) \\ p &\in D_{\mathbb{M}} \subset \mathbb{R}^d \end{aligned} \tag{2.6}$$

where $e(t)$ is white noise with PDF denoted by $f_e(x, p)$, and d is the dimension of vector p. It is worth to note that (2.6) is *a set of models* and then the identification method is utilized to find the model which is the most appropriate one according to the specific application at hand. Considering $G(q, p)$ as the discrete-time version of the system transfer function, (2.6) can be written in *one-step-ahead-prediction* form by knowing the values of $u(s)$ and $y(s)$ for $s \leq t-1$ as

$$\hat{y}_1(t|p) = H^{-1}(q, p)G(q, p)u(t) + [1 - H^{-1}(q, p)]y(t) \tag{2.7}$$

where $\hat{y}_1(t|p)$ is *one-step-ahead-predictor* of the output which is dependent on the unknown parameter vector p. Notice that the predictor representation in (2.7) does not depend on the PDF of $e(t)$. Now we have a parametrized set of models which is called a model structure $\mathbb{M}$ and consequently $\mathbb{M}(p)$ is a specific model which is determined using a specific parameter vector p.

State-space equations use state variables to describe a model by a system of first-order Ordinary Differential Equations (ODE) or difference relations, rather than a system of nth-order differential or difference equations. State variables $x(t)$ can be reconstructed from the measured input and output data, but usually they are not directly measured during an experiment. As an example, a parametrized linear continuous-time state-space structure $\mathbb{M}$ with $m \times 1$ input vector $u(t)$, $k \times 1$ output vector $z(t)$, and $n \times 1$ state vector $x(t)$ is

$$\begin{aligned} \dot{x}(t) =& A(p)x(t) + B(p)u(t) \\ z(t) =& C(p)x(t) \\ y(t) =& z(t) + v^*(t) \end{aligned} \tag{2.8}$$

where $y(t)$ is $k \times 1$ vector denoted as output measurement at desired sampling instants subjected to an additive noise $v^*(t)$ term. Notice that the parameters p might enter the model in a nonlinear way. So the model can be linear in the states but nonlinear in the parameters. If $v^*(t)$ is white noise, (2.8) is called an Output Error (OE) model structure and $H(q, p) = 1$ in (2.6). However, if it is required to model the characteristics of the noise term $v^*(t)$, a noise model $H(q, p) \neq 1$ should be applied. The continuous-time formulation of (2.8) can be transported to the corresponding discrete-time representation in several ways,

such as simple Euler approximation, see Gustafsson et al. (2010). Most often, the noise term $v^*(t)$ is proposed with the process noise $w(t)$ and measurement noise $v(t)$, as in

$$\begin{aligned} x(t+1) =& A_D(p)x(t) + B_D(p)u(t) + w(t) \\ y(t) =& C(p)x(t) + v(t) \end{aligned} \tag{2.9}$$

where subscript D stands for discrete-time and $w(t)$ and $v(t)$ are sequences of independent random variables with zero mean and are given by their covariances, $R_1(p)$ and $R_2(p)$ respectively. The one-step-ahead-prediction form of the state-space formulation (2.9) in *innovations form* can be written as, see Kalman (1960),

$$\begin{aligned} \hat{x}(t+1,p) =& A_D(p)\hat{x}(t,p) + B_D(p)u(t) + K(p)\varepsilon(t) \\ y(t) =& C(p)\hat{x}(t,p) + \varepsilon(t) \end{aligned} \tag{2.10}$$

where $\hat{y}_1(t|p) = C(p)\hat{x}(t,p)$ is the model one-step-ahead predictor and $\varepsilon(t)$ is the prediction-error which is the part of $y(t)$ that cannot be predicted from past measurements. The feedback matrix $K(p)$ is given as

$$K(p) = \left[A_D(p)\bar{P}(p)C^{\mathrm{T}}(p) + R_{12}(p)\right]\left[C(p)\bar{P}(p)C^{\mathrm{T}}(p) + R_2(p)\right]^{-1} \tag{2.11}$$

where $E\, w(t)v^{\mathrm{T}}(t) = R_{12}(p)$ is the cross covariance between process noise $w(t)$ and measurement noise $v(t)$. $\bar{P}(p) = \bar{E}[x(t) - \hat{x}(t,p)][x(t) - \hat{x}(t,p)]^{\mathrm{T}}$ is the covarinace of the state estimate error and is obtained as the positive semi-definite solution of the stationary Riccati equation

$$\begin{aligned} &\bar{P}(p) = A_D(p)\bar{P}(p)A_D^{\mathrm{T}}(p) + R_1(p) - \left[A_D(p)\bar{P}(p)C^{\mathrm{T}}(p) + R_{12}(p)\right] \\ &\times \left[C(p)\bar{P}(p)C^{\mathrm{T}}(p) + R_2(p)\right]^{-1}\left[A_D(p)\bar{P}(p)C^{\mathrm{T}}(p) + R_{12}(p)\right]^{\mathrm{T}}. \end{aligned} \tag{2.12}$$

Using the forward shift operator q, (2.10) can be written in the form (2.6) in which $G(q,p)$ and $H(q,p)$ are defined as follows

$$\begin{aligned} G(q,p) =& C(p)[qI - A_D(p)]^{-1}B_D(p) \\ H(q,p) =& C(p)[qI - A_D(p)]^{-1}K(p) + I. \end{aligned} \tag{2.13}$$

For a linear OE model structure, in which no process noise $w(t)$ exists, the feedback terms $K(p)$ in (2.10) are zero. However, for modeling the engine-load system in this thesis the process noise is present to compensate for uncertainty in model structure and consequently the feedback terms $K(p)$ are not zero.

The next section will be devoted to the question of how a suitable model $\mathfrak{m} = \mathbb{M}(\hat{p})$ can be defined, or in other words how the model unknown parameters vector p can be estimated. This is the task of identification method.

2.2.2 Identification method

Having a model structure $\mathbb{M}$ for the dynamic system $\mathbb{S}$, it is now the time to estimate a model $\mathfrak{m} = \mathbb{M}(\hat{p})$ that is reliable for the purpose of application. The N-points input and output data set $Z^N = [y(1), u(1), y(2), u(2), ..., y(N), u(N)]$ has been collected from the system $\mathbb{S}$ and are going to be used to find the best value for $\hat{p}$. The mathematical structure of a dynamic system is not always known, therefore in these applications *black-box* modeling is used in which the output is written as a polynomial of previous inputs, outputs, and the noise term. The order of the model depends on how many time shifts are included, see Gustafsson et al. (2010). However, as noted in Section 2.2.1, in this thesis the mathematical structure of the engine-load system is known since it is assumed that the true system can be given by a state-space formulation as in (2.9), see also representation (3.13) in modeling Chapter 3. Accordingly, there exists a known model structure with the vector of unknown parameters p to be estimated which has physical interpretation, see Section 2.2.1. That's the reason to call this identification approach, *grey-box* modeling. Moreover, if the covariance of $w(t)$ and $v(t)$ are not known, a direct parametrization of the feedback vector $K(p)$ can be used to estimate its coefficients simultaneously with the other unknown model parameters. This approach is called *Parametrized Observer* (PO) method, see Larsson et al. (2009). As mentioned in Section 2.2.1, the linear state-space model (2.10) can be nonlinear in parameters, which is the case in our application.

Prediction-error method

The prediction-errors of a specific model structure $\mathbb{M}(p)$ can be calculated as, see (2.10),

$$\varepsilon(t, p) = y(t) - \hat{y}_1(t|p) \tag{2.14}$$

and thus, by having the input and output data set Z^N, (2.14) can be computed for time instants $t = 1...N$. A good model is the one which possesses as small prediction-errors as possible. The *Prediction-Error Method* is based on the technique which minimizes the prediction-errors $\varepsilon(t, p)$ with respect to the model parameters p, see Ljung (1999). Generally, this can be formulated as an unconstrained optimization problem with the scalar cost function

$$V_N(p, Z^N) = \frac{1}{N} \sum_{t=1}^{N} l(L(q)\varepsilon(t, p)) \tag{2.15}$$

where $L(q)$ is a linear stable filter with q being the forward shift operator and l is a scalar-valued (typically positive) function. For simplicity, in this thesis $L(q) = 1$ and $l = \frac{1}{2}\varepsilon(t, p)^{\mathrm{T}}\varepsilon(t, p)$ are selected. Therefore the minimization of loss function given in (2.15), with the mentioned choices of $L(q)$ and l, can be

represented as follows

$$\hat{p}_N = \arg\min_{p \in D_{\mathbb{M}}} V_N(p, Z^N) \tag{2.16}$$
$$V_N(p, Z^N) = \frac{1}{N} \sum_{t=1}^{N} \frac{1}{2} \varepsilon(t,p)^{\mathrm{T}} \varepsilon(t,p).$$

If the predictor $\hat{y}(t|p)$ of a model can be written as a scalar multiplication of a known data vector $\phi(t)$ containing past inputs and outputs, and the parameter vector p, the model is named as *linear regression* in statistics and $\phi(t)$ is called the regression vector. Using the quadratic criterion for loss function of this regression problem, there exists an analytical solution for $\hat{p}_N$ in (2.16) which is called *Least-Squares Estimate* (LSE)

$$\hat{p}_N^{(\mathrm{LSE})} = (\Phi^{\mathrm{T}}\Phi)^{-1}\Phi^{\mathrm{T}} y \tag{2.17}$$

where $\Phi = [\phi_1 \ \phi_2 \ ... \ \phi_N]^{\mathrm{T}}$. However, in the general case the optimization problem (2.16) cannot be solved analytically. Then it is required to have a numerical iterative search technique in which the value of loss function $V_N(p, Z^N)$ improves in each step. A general type of search method is

$$\hat{p}_N^{(i+1)} = \hat{p}_N^{(i)} - \mu_N^{(i)} [R_N^{(i)}]^{-1} V_N'(\hat{p}_N^{(i)}, Z^N) \tag{2.18}$$

where i denotes the iteration number and $\mu_N^{(i)}$ is the step length that should be selected in a way that the loss function $V_N(p, Z^N)$ decreases with increasing iterations. $R_N^{(i)}$ is responsible for modifying the search direction and depending on how this term is chosen different methods are obtained, namely, gradient or steepest-descent, Newton, Gauss-Newton, and Levenberg-Marquardt methods. Considering the $\varepsilon(t,p)$ in (2.14) and $\psi^{\mathrm{T}}(t,p) = -\frac{d}{dp}\varepsilon(t,p)$, the corresponding $R_N^{(i)}$ for each of these methods is

- Steepest-descent
$$R_N^{(i)} = I \tag{2.19}$$

- Newton
$$R_N^{(i)} = V_N''(p_N^{(i)}, Z^N) \tag{2.20}$$
in which
$$V_N''(p_N^{(i)}, Z^N) = \frac{1}{N} \sum_{t=1}^{N} \psi(t, p_N^{(i)}) \psi^{\mathrm{T}}(t, p_N^{(i)}) - \frac{1}{N} \sum_{t=1}^{N} \psi'(t, p_N^{(i)}) \varepsilon(t, p_N^{(i)}) \tag{2.21}$$

- Gauss-Newton
$$R_N^{(i)} = \frac{1}{N} \sum_{t=1}^{N} \psi(t, p_N^{(i)}) \psi^{\mathrm{T}}(t, p_N^{(i)}) \tag{2.22}$$

- Levenberg-Marquardt (Regularization technique)

$$R_N^{(i)(\lambda)} = \frac{1}{N}\sum_{t=1}^{N}\psi(t,p_N^{(i)})\psi^{\mathrm{T}}(t,p_N^{(i)}) + \lambda I \tag{2.23}$$

  where λ is used for regularization and if it is set zero, the last two procedures are the same. However, the Levenberg-Marquardt has an advantage in comparison to Gauss-Newton in the circumstances that (2.22) is singular or close to be. This may happen if the model is over-parametrized or the data is not sufficiently informative. Using regularization techniques with the aid of λ factor will be a remedy to this singularity issue.

In this thesis, `greyest` function in Matlab System Identification Toolbox is applied for parameter estimation of the continuous-time LTI model (3.13) representing the engine-load system. Note that the `greyest` command accepts the system matrices in continuous-time format and utilizes PEM besides a combination of different search algorithms mentioned in (2.19)-(2.23) when the `'auto'` option is chosen.

Remarks on identifiability analysis

A fundamental question, before operating any estimation procedure, is whether the model is identifiable or not. This question contains two sub-problems. The first concerns about the data characteristics which studies if the data is sufficiently informative to distinguish between different models. The second issue is about the *invertibility of model structure* $\mathbb{M}$ that investigates the possibility of uniquely determining (locally or globally) the model parameters from a data set which is assumed to be informative enough. The latter problem is called *structural identifiability*. Three definitions are given in the sequel related to such invertibility characteristics based on the discussion in Ljung (1999).

Definition 2.*a* A model structure $\mathbb{M}$ is globally identifiable at p^* if

$$\mathbb{M}(p) = \mathbb{M}(p^*), \quad p \in D_{\mathbb{M}} \Rightarrow p = p^*. \tag{2.24}$$

After describing identifiability at one point, the properties of the whole set is studied:

Definition 2.*b* A model structure $\mathbb{M}$ is *strictly* globally identifiable at p^* if it is globally identifiable at all $p^* \in D_{\mathbb{M}}$.

Having these two definitions, the corresponding *local properties* can be defined similarly.

Definition 2.*c* A model structure $\mathbb{M}$ is locally identifiable at p^*, if there exist an ϵ such that

$$\mathbb{M}(p) = \mathbb{M}(p^*), \quad p \in B(p^*,\epsilon) \Rightarrow p = p^* \tag{2.25}$$

where $B(p^*,\epsilon)$ is an $\epsilon-$neighborhood of p^*.

A huge amount of literature has been devoted to the problem of structural identifiability for linear and nonlinear state-space models, see Hermann and Krener (1977); Walter (1982); Ollivier (1989); Ljung and Glad (1994); Sedoglavic (2002); Anguelova (2007); Karlsson et al. (2012). Unfortunately, computational complexity of some well-known methods, such as characteristic set determination, increases exponentially with the number of states and the unknown parameters, see Ollivier (1989); Ljung and Glad (1994). Therefore, as presented in Sedoglavic (2002); Anguelova (2007), the model structural identifiability can be studied by using the so-called rank-test method which is basically similar to observability investigation. This approach will be briefly discussed here. By neglecting the effect of additive noise $v^*(t)$, the linear state-space model (2.8) can be written as follows

$$\begin{aligned} \dot{x}(t) =& A(p)x(t) + B(p)u(t) \\ y(t) =& C(p)x(t) \end{aligned} \tag{2.26}$$

where $x \in \mathbb{R}^n$, $u \in \mathbb{R}^m$, and $y \in \mathbb{R}^k$ are the state, the input, and the output vectors, respectively. The structural identifiability problem can be defined as observability of the extended nonlinear system, see Walter (1982),

$$\begin{aligned} \begin{bmatrix} \dot{x} \\ \dot{p} \end{bmatrix} &= \begin{bmatrix} f(x,u,p) \\ 0 \end{bmatrix} = \zeta^0(x,p) + \zeta(x,p)u \\ y &= \eta(x,p) = \begin{bmatrix} \eta_1(x,p) \ \dots \ \eta_k(x,p) \end{bmatrix}^{\mathrm{T}}. \end{aligned} \tag{2.27}$$

To prove observability of the nonlinear system given in (2.27), i.e. the initial states can be reconstructed from data, the following system of equations should be solved for x and p, where the input and output and their time derivatives are assumed to be available.

$$\begin{aligned} y_1^{(0)} &= \eta_1^{(0)}(x,p) \\ y_1^{(1)} &= \eta_1^{(1)}(x,p,u_1,\dots,u_m) \\ &\vdots \\ y_1^{(\kappa)} &= \eta_1^{(\kappa)}\big(x,p,u_1,\dots,u_1^{(\kappa-1)},\dots,u_m,\dots,u_m^{(\kappa-1)}\big) \\ &\vdots \\ y_k^{(0)} &= \eta_k^{(0)}(x,p) \\ y_k^{(1)} &= \eta_k^{(1)}(x,p,u_1,\dots,u_m) \\ &\vdots \\ y_k^{(\kappa)} &= \eta_k^{(\kappa)}\big(x,p,u_1,\dots,u_1^{(\kappa-1)},\dots,u_m,\dots,u_m^{(\kappa-1)}\big). \end{aligned} \tag{2.28}$$

The notations $(.)^{(i)}$ in (2.28) means the ith time derivative of $(.)$. If, for a given κ, the derivative array system of equations in (2.28) can be solved uniquely for

the parameters p, the system is observable and therefore identifiable. However, for a general nonlinear system, no upper limit exists for κ and thus it could be infeasible to solve this system. As a remedy, the nonlinear system of equations in (2.28) can be linearized around the extended states and the Jacobian is studied to determine the model local observability, see Hermann and Krener (1977),

$$\mathbb{O}(x,p,u_1,\ldots,u_m^{(\kappa-1)}) = \begin{bmatrix} \frac{\partial \eta_1^{(0)}(x,p)}{\partial(x,p)} \\ \frac{\partial \eta_1^{(1)}(x,p,u_1,\ldots,u_m)}{\partial(x,p)} \\ \vdots \\ \frac{\partial \eta_1^{(\kappa)}\left(x,p,u_1,\ldots,u_1^{(\kappa-1)},\ldots,u_m,\ldots,u_m^{(\kappa-1)}\right)}{\partial(x,p)} \\ \vdots \\ \frac{\partial \eta_k^{(0)}(x,p)}{\partial(x,p)} \\ \frac{\partial \eta_k^{(1)}(x,p,u_1,\ldots,u_m)}{\partial(x,p)} \\ \vdots \\ \frac{\partial \eta_k^{(\kappa)}\left(x,p,u_1,\ldots,u_1^{(\kappa-1)},\ldots,u_m,\ldots,u_m^{(\kappa-1)}\right)}{\partial(x,p)} \end{bmatrix}. \tag{2.29}$$

The matrix $\mathbb{O}(x,p,u_1,\ldots,u_m^{(\kappa-1)})$ in (2.29) is called the *extended observability matrix* and can be evaluated in a specific operating point x^*, see Linder et al. (2014). The system is *locally weakly identifiable* if $\mathbb{O}$ meets the observability rank condition, see Hermann and Krener (1977); Anguelova (2007). If the system (2.27), i.e. ζ^0, ζ, and η, are rational functions of their arguments, it is enough to consider the first $\kappa = n + d - 1$ derivatives of $\eta_j(x,p),\ j = 1 \ldots k$, where d is the number of unknown parameters, i.e. size of vector p. This has been proved in Anguelova (2007). Weak local structural identifiability of the system (2.26) is tested with a rank condition on $\mathbb{O}$.

The symbolic calculations for obtaining the matrix $\mathbb{O}$ contain repeated Lie-derivatives computations which may become highly complex when it comes to higher order systems. In Sedoglavic (2002), a probabilistic semi-numerical approach has been proposed to directly calculate the Jacobian $\mathbb{O}$ which is more suitable for large systems even up to a few hundred states and parameters. A Mathematica implementation of this method has been introduced in Karlsson et al. (2012). It is a ready to use package named `IdentifiabilityAnalysis` and is available by the authors. Consequently, in Chapter 4 the procedure of symbolic calculations is performed in detail to study the structural identifiability of the simplified 2 DOF state-space model structure, which has three states, with only one unknown parameter to avoid big size and complexity. After illustrating the method for the smaller system, the symbolic software is used to calculate the rank of observability matrix $\mathbb{O}$ for the 2 DOF model but instead with five unknown parameters simultaneously. The rank test shows it is possible to identify all five parameters of the 2 DOF model assuming informative inputs. Finally, the

structural identifiability of the unknown parameters in the 7 DOF engine-load system (3.13), which has 13 states, is investigated using the Mathematica package which was mentioned above. Again the rank test proves that all the unknown parameters of the 7 DOF model structure are identifiable having informative inputs.

As mentioned in the beginning of this section, the structural identifiability is one leg of the identifiability problem. The second leg is related to data information. A big value of estimated variance for a specific parameter in the model structure is a sign of low sensitivity of the model predictor to this parameter for the current data set. This means the parameter cannot be estimated correctly even if it is structurally identifiable in the first place. Hence, to have a reliable estimation, the input $u(t)$ and the output $y(t)$ are chosen in a way that the predicted output turns to be sensitive to the parameters which are important for the application at hand. In other words, the selected data should have the required information about the considered parameters. As an example, in Chapter 4 it is illustrated that changing the data set from normal combustion data set to a data set which has misfire in the input torque from the engine, will help estimate the unknown parameters of the engine-load system.

2.2.3 Model validation

The identification steps, which have been introduced so far, find the best model $\mathfrak{m} = \mathbb{M}(\hat{p}_N)$ inside the current model structure, see (2.7). In the grey-box modeling approach, it is important to check whether the estimated physical parameters are in a reasonable range besides that their estimated variances are not considerably large. This is the first validation test. Further, the model quality should be validated using a data set, called *validation data*, which is different from the one applied for building the model named *estimation data*. This is to show that the model is applicable in general, i.e. the model fit is good for all possible data sets from the system and not just for the specific data set which has been used during estimation. Such validation is called *cross-validation* and is performed in two steps: the first is to study the model fit for predicted and simulated outputs, and the second is to do residual analysis. Theses aspects are described in the following sections.

Model fit

How much the estimated model $\mathfrak{m}$ is able to reproduce the validation data set from the true system is the first basic question that should be answered. Two different kinds of model outputs are calculated here: the one-step-ahead-predictor $\hat{y}_1(t|\mathfrak{m})$ as in (2.7) and the simulated output $\hat{y}_s(t|\mathfrak{m})$. The latter is the case where the prediction horizon k is equal to ∞. Having the values of $u(s)$ and $y(s)$ for $s \leq t-k$, the k-step-ahead-predictor of the linear model $\mathfrak{m}$ at time instance

t is denoted by $\hat{y}_k(t|\mathfrak{m})$, and can be computed as follows, see (2.7),

$$\begin{aligned} \hat{y}_k(t|\mathfrak{m}) &= W_k(q,\hat{p})G(q,\hat{p})u(t) + [1 - W_k(q,\hat{p})]y(t) \\ W_k(q,\hat{p}) &= \bar{H}_k(q,\hat{p})H^{-1}(q,\hat{p}) \\ \bar{H}_k(q,\hat{p}) &= \sum_{l=0}^{k-1} h(l,\hat{p})q^{(-l)} \end{aligned} \tag{2.30}$$

where as always q is forward shift factor and $G(q,\hat{p})$ and $H(q,\hat{p})$ are the system and the noise transfer functions for the estimated model $\mathfrak{m}$, see (2.6) and (2.13). If $k = \infty$, $\bar{H}_k(q,\hat{p}) = H(q,\hat{p})$ and consequently $W_k(q,\hat{p}) = 1$ which according to (2.30) results in a pure simulation

$$\hat{y}_s(t|\mathfrak{m}) = G(q,\hat{p})u(t) \tag{2.31}$$

where only the past inputs are used. It is worth to remind that for OE models $H(q) = 1$, as mentioned in Section 2.2.1, and thus there is no difference between one-step-ahead-predictor $\hat{y}_1(t|\mathfrak{m})$ and simulated output $\hat{y}_s(t|\mathfrak{m})$ considering relations (2.7) and (2.31). It is important to keep in mind that there can be a very good agreement between $\hat{y}_1(t|\mathfrak{m})$ and $y(t)$, since the previous values of output, i.e. $y(s)$, $s \leq t-1$, are used. This is not the case for $\hat{y}_s(t|\mathfrak{m})$ which no previous output values are applied and therefore it can be more revealing since the output is built from input only. Of course for an unstable model, the predictor form should be used. In this thesis, all the comparisons are made between the model simulated output and the measured system data.

The fit of the estimated model $\mathfrak{m}$ can be shown by comparison plots or a value $F(\mathfrak{m}, Z^N)$ which is computed as follows

$$F(\mathfrak{m}, Z^N) = 100\left(1 - \frac{\sqrt{\frac{1}{N}\sum_{t=1}^{N}|y(t) - \hat{y}_s(t|\mathfrak{m})|^2}}{\sqrt{\frac{1}{N}\sum_{t=1}^{N}|y(t) - \bar{y}(t)|^2}}\right) \tag{2.32}$$

in which $\bar{y}(t)$ is the output mean.

Residual analysis

The *residuals* or leftovers are the part of the true system which are not reconstructed by the model. There exists information about the model quality in the corresponding residuals. Having found the model $\mathfrak{m} = \mathbb{M}(\hat{p}_N)$, the residual for each time instant t can be computed as following, see (2.10),

$$\varepsilon(t) = \varepsilon(t,\hat{p}_N) = y(t) - \hat{y}_s(t|\hat{p}_N). \tag{2.33}$$

Now, having a validation data set $Z^N = [y(1), u(1), y(2), u(2), ..., y(N), u(N)]$, the first point that can be considered is to obtain the maximum residual S_1

produced by the model $\mathbb{M}$ in the desired time interval or calculating the average error S_2

$$S_1 = \max_t |\varepsilon(t)|,\ S_2^2 = \frac{1}{N}\sum_{t=1}^{N}\varepsilon^2(t). \tag{2.34}$$

However, one may ask a very basic question here: how likely is that these values are not changing for future data sets? Answering this question requires to confirm that the residuals do not depend on something which is probable to change. One clear example is their independency from special input given in Z^N. This can be acquired by looking at the *cross covariance* between the past inputs and the residuals

$$\hat{R}^N_{\varepsilon u}(\tau) = \frac{1}{N}\sum_{t=1}^{N}\varepsilon(t)u(t-\tau). \tag{2.35}$$

The small values of $\hat{R}^N_{\varepsilon u}(\tau)$ is a positive sign that if this model is applied to some other inputs, the measures given in (2.34) are still applicable. There exists another important expression that can be concluded if the values of $\hat{R}^N_{\varepsilon u}(\tau)$ are not small: some parts of $y(t)$ which come from the past inputs are not appropriately reconstructed by the model $\mathbb{M}$. Therefore, the model can be still improved.

Correlations among the residuals themselves should be also investigated

$$\hat{R}^N_{\varepsilon}(\tau) = \frac{1}{N}\sum_{t=1}^{N}\varepsilon(t)\varepsilon(t-\tau). \tag{2.36}$$

If $\hat{R}^N_{\varepsilon}(\tau)$ are not small for $\tau \neq 0$, there is a trace of previous $\varepsilon(t)$ in the current value and this proves that $y(t)$ could have been predicted better and thus the model $\mathbb{M}$ should be improved.

As mentioned in the beginning of this chapter, the third step in the identification procedure happens when the identified model cannot pass the validation tests described in Section 2.2.3. Consequently the first two steps should be repeated until sufficient confidence about the model is gained.

2.3 A SIMPLE EXAMPLE

Now having introduced what is a dynamic system and how a system identification procedure can be performed, an illustrative example is given in this section. The considered structure is a simple torsional mass-damper system which is shown in Figure 2.3 and can represent the simplified version of a four-cylinder IC engine configuration, i.e. damping wheel, four cylinders, and flywheel, see Figure 3.6 in Chapter 3. The aim is to identify a model that can be used to describe the angular velocity $\dot{\theta}_\mathrm{e}$ of the rotating mass J_e, given in Figure 2.3, applying an input torque T_e from the engine. Defining the state $x_\mathrm{e} = \dot{\theta}_\mathrm{e}$ and using the Newton's

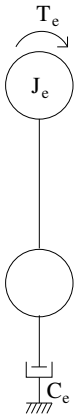

Figure 2.3: *Simplified version of a crankshaft system.*

second law, the model structure for this system in state-space form (2.8) can be written as

$$\begin{aligned} \dot{x}_{\mathrm{e}}(t) &= \frac{1}{J_{\mathrm{e}}}\Big(- C_{\mathrm{e}} x_{\mathrm{e}}(t) + T_{\mathrm{e}}(t)\Big) \\ y(t) &= x_{\mathrm{e}}(t) + v_{\mathrm{e}}(t) \end{aligned} \tag{2.37}$$

in which C_{e} is the friction coefficient modeled as viscous damping, $y(t)$ is the measured output which is angular velocity, and $v_{\mathrm{e}}(t)$ is assumed to be white noise with zero mean and standard deviation 0.1 rad/sec. J_{e} and C_{e} are the unknown model parameters to be estimated using an available input and output data set Z^N_{est} shown in Figure 2.4. To confirm the applicability of the identified model, it needs to be validated against another data set Z^N_{val}. In this example these data sets are generated by simulation, however in real engine-load test they are measured. The true values for the parameters are assumed to be $J_{\mathrm{e}} = 0.3635$ and $C_{\mathrm{e}} = 0.1532$.

The discretized model structure (2.37), by using a simple Euler forward approach and a sampling time $T_{\mathrm{s}} = 0.01$s, is

$$x_k = (1 + T_{\mathrm{s}}\alpha)x_{k-1} + T_{\mathrm{s}}\beta\, T_{\mathrm{e},k-1} \tag{2.38}$$

where $\alpha = -C_{\mathrm{e}}/J_{\mathrm{e}}$ and $\beta = 1/J_{\mathrm{e}}$. It is seen that the model predictor defines a linear regression problem and thus the predictor of $y(t)$ in (2.37) in discrete-time can be written as

$$\begin{aligned} \hat{y}_k(p) &= \phi_k^{\mathrm{T}} p_e, \\ \phi_k &= [x_{k-1} \;\; T_{\mathrm{e},k-1}]^{\mathrm{T}}, \\ p_e &= [(1 + T_{\mathrm{s}}\alpha) \;\; T_{\mathrm{s}}\beta]^{\mathrm{T}} \end{aligned} \tag{2.39}$$

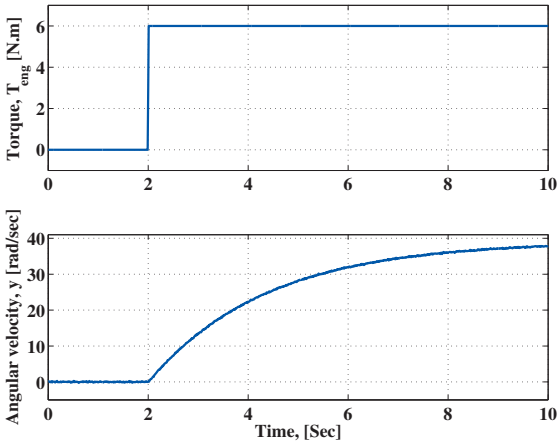

Figure 2.4: *Estimation data* Z^N_{est}. *A white noise with zero mean and standard deviation* 0.1 *rad/sec is added to simulated* x_k *to generate output* y_k.

in which ϕ_k is the regression vector and p_e is the vector of unknown parameters. Now, the LSE in (2.17) gives the estimated vector of parameters $\hat{p}_e$ and consequently, using (2.39), $\hat{J}_{\mathrm{e}}^{\mathrm{LSE}} = 0.3571$ and $\hat{C}_{\mathrm{e}}^{\mathrm{LSE}} = 0.1500$ are obtained for the model structure (2.37). After estimating the unknown parameters using estimation data, the model should be validated which consists of two steps: model fit and residual analysis. A fresh data set Z^N_{val} is applied for validation in which a sine input is considered. Figure 2.5 shows the simulated angular velocity, using (2.31), versus the true system. As it is seen there is a good agreement between the model and the new data in which the fit value $F(\mathfrak{m}, Z^N) = 85.32\%$ is calculated using (2.32). Moreover, the correlations among the residuals and the cross covariance between the past inputs and residuals are given in Figure 2.6 where almost all the values are inside 99% confidence interval. According to Section 2.2.3, it can be said that the residuals do not depend on something which is probable to change.

The next chapter is devoted to the torsional vibration modeling of an engine-load configuration which is the dynamic system of interest in this thesis. In comparison to the simple example given in Section 2.3, this considered system is more complicated since there will be more states which are not measured. Furthermore, the unknown parameters will enter the state-space equations in a nonlinear way and thus the linear regression predictor is not applicable anymore.

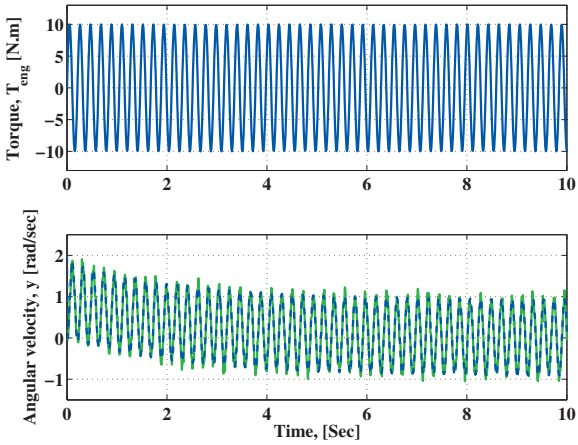

Figure 2.5: *Validation data Z_{val}^N. The estimated model (dashed line) and the true system (solid line).*

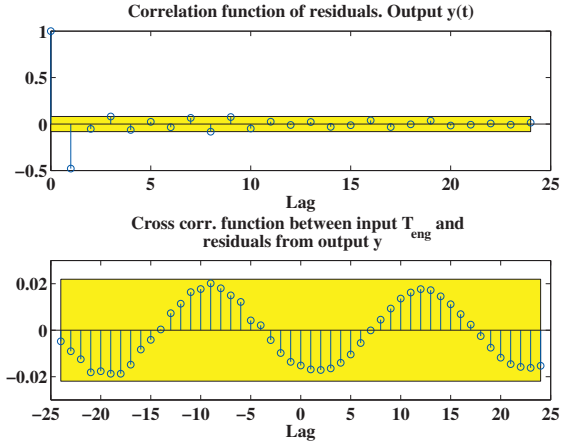

Figure 2.6: *Residual analysis using data set Z_{val}^N*

Chapter 3

Engine-load system torsional vibration modeling

"Make your theory as simple as possible, but no simpler."
- Albert Einstein (1879 - 1955)

The main source of excitation forces in a vehicle engine structure and, consequently, its powertrain system arises from the crankshaft vibrations due to the oscillatory engine torque. These vibrations occur in three dimensional space and are therefore of different types: bending, axial, and torsional. Moreover, they include separate frequency ranges. In this chapter, a mathematical model which is capable of reproducing torsional behavior of an engine-load system will be developed and explained. A four-cylinder four-stroke IC engine, which is shown in Figure 3.1, is studied. The considered engine is spark ignited which is nowadays a widely used engine in passenger cars and motorbikes. Since the main focus of this thesis is the engine-load system torsional vibration modeling, the rotational dynamics of the engine is considered by modeling the crankshaft while the other parts, such as engine mounts, are not taken into consideration.

3.1 Crankshaft model

The major torsional vibrations of a crankshaft system are due to discrete engine ignition events, in other words, the fluctuating nature of the delivered engine torque. Crankshaft systems can be modeled by torsional elastic elements. The actual system is distributed, but basic models comprise linear lumped spring-mass-damper systems which, according to the specific purpose of modeling, can be extended by additional details about the dynamics of various parts. As described in Rabeih (1997), the compact crankshaft is very stiff, and hence each crank-slider mechanism, which is shown in Figure 3.2, can be represented by one inertia disc J_i. Each J_i consists of the reciprocating masses inertias J_r,

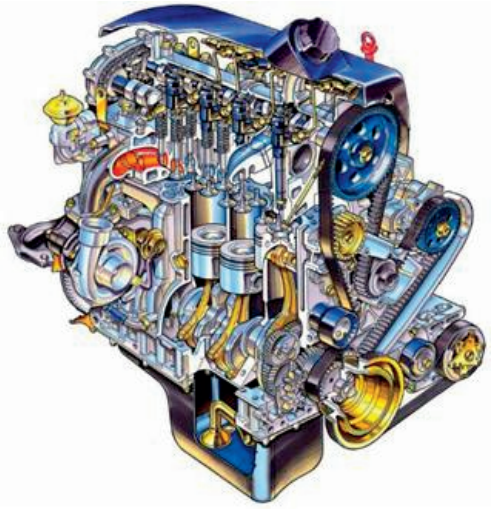

Figure 3.1: *Four-cylinder spark ignited internal combustion engine, (Reproduced with permission from www.car-engineer.com, Nicolas (2012)).*

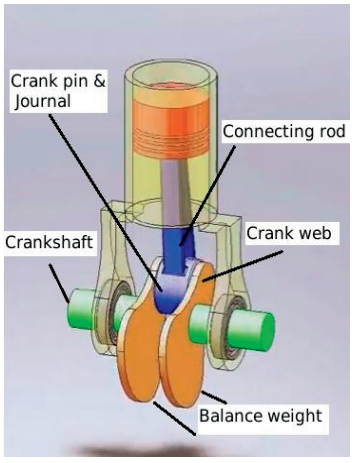

Figure 3.2: *Crank-slider mechanism, see Ranjan (2011).*

i.e., piston and connecting rod, plus the inertias of the rotating parts J_w, i.e. crank journal, crank pin, crank web, and balance weight. The crank front view and the crank-slider mechanism equivalent structure are depicted in Figure 3.3. Considering the damping wheel inertia disc at the free end of the crankshaft, left side, and the flywheel inertia disc at the other end, right side, the crankshaft model for the four-cylinder IC engine, shown in Figure 3.1, is given in Figure 3.4. The inertias are connected with torsional stiffness coefficients $K_{i+1,i}$.

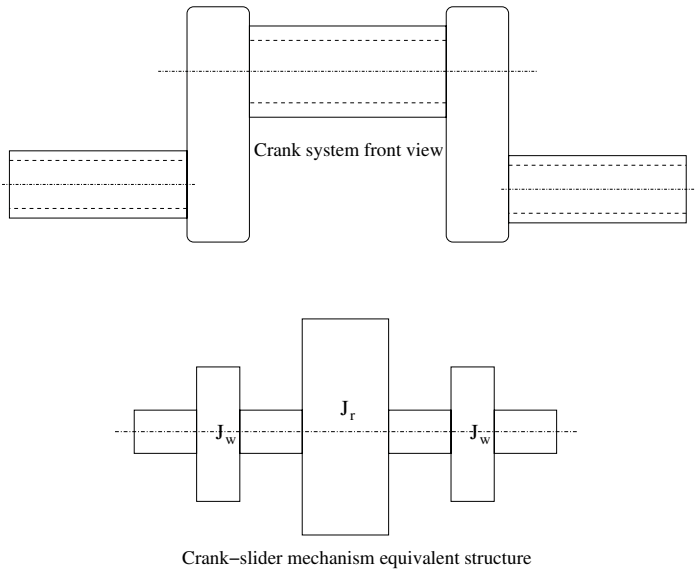

Figure 3.3: *Crank and crank-slider mechanism original and equivalent systems.*

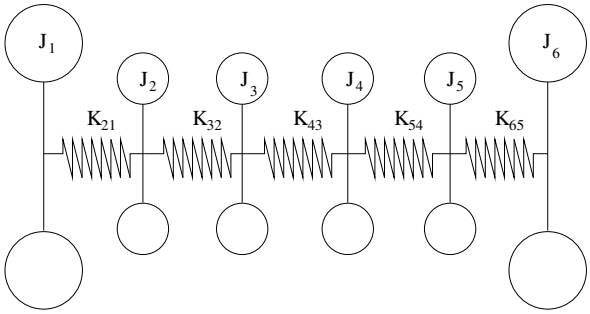

Figure 3.4: *Crankshaft model for a four-cylinder IC engine.*

3.1.1 Damping and engine friction modeling

Damping is present in all vibrating systems and its functionality is to dissipate energy. An accurate mathematical form describing damping force for a given mechanical system is complicated. However in most of the applications the following simplified models are sufficient, see Liu and Huston (2011),

- A damping force which is proportional to the velocity is called viscous damping. The applied force is due to the inertia of a viscous fluid which results in a resistance for movement during pouring or a sudden shift. If this fluid is used between two surfaces that are rapidly turned in opposite directions, the liquid will resist this turning motion induced by the shear

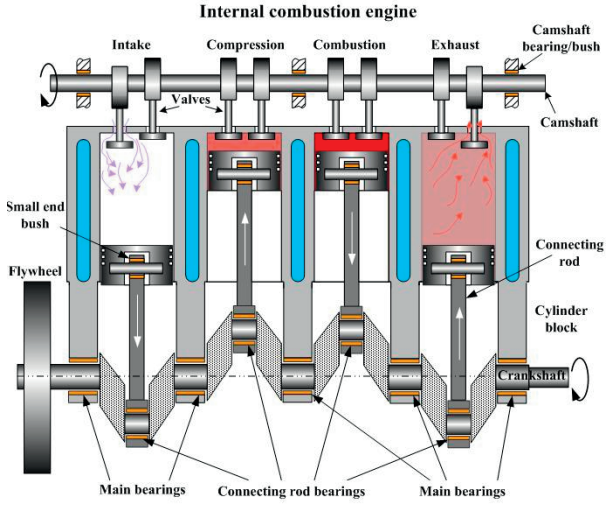

Figure 3.5: *The rotating and reciprocating parts of an IC engine in which bearing points illustrate the places exposing relative motions of solid bodies, (Reproduced with permission from www.substech.com, Kopeliovich (2014)).*

force. Any of these phenomena can be applied in a viscous damper.

- Depending on the application, the damping force can be proportional to the squared velocity, such as turbulent friction in a fluid column oscillating within a U-tube, see Richardson (1963).
- Coulomb damping which is typically due to dry friction, see Dowson (1998).
- Structural (hysteresis) damping which is attributed to internal friction in structure materials.

As mentioned by Sandoval and Heywood (2003), the total engine friction originates from different sources, see also Soltic (2000). The segmentation and magnitude of each friction source depend on various engine characteristics, namely, structure, age, operating point (load and speed), and temperature of components and lubricants. Therefore, engine friction modeling is a complicated task and one remedy is to analyze different friction mechanisms, which are present at different parts of the running engine, separately. Considering the first damping phenomenon mentioned above, viscous damping law can be applied for all the crankshaft system components which are featured to relative motion of two surfaces having an oil film in between, such as journal bearings and piston-rod-crank units. Figure 3.5 depicts the rotating and reciprocating parts of an IC engine with the points denoted by *bearing* where relative motions of solid bodies occur. According to Figure 3.5, a viscous damping coefficient $C_{i+1,i}$ can be used in the connection of two consecutive inertias, J_i and J_{i+1} in

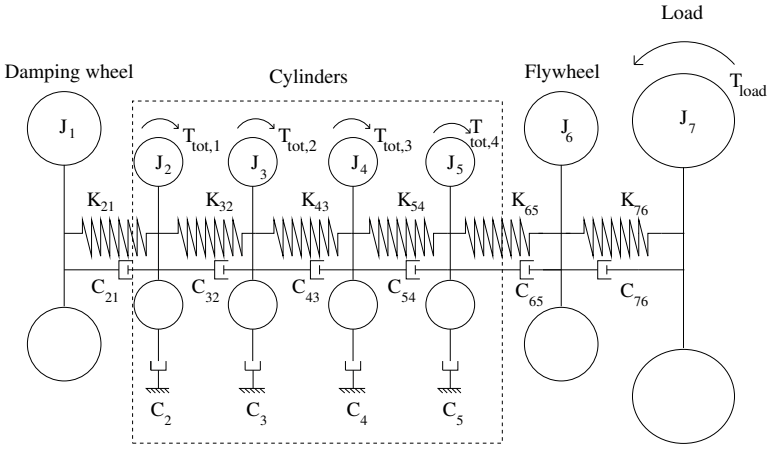

Figure 3.6: 7 *DOF lumped torsional vibration model of a four-cylinder SI engine-load configuration.*

Figure 3.4. This is to represent the damping torque arising from rotation of the crankshaft on its journal bearing. Moreover, the equivalent viscous torsional damping torque for each piston-rod-crank unit is represented by C_i for each inertia J_i, $i = 2, \cdots, 5$, see Figure 3.4. In this thesis, the hysteresis damping of the crankshaft components and dry friction damping are neglected.

3.1.2 Overall engine-load system model

Obeying the same rule as in Section 3.1, the brake system can also be modeled by an extra lumped inertia connected to the flywheel through a flexible coupling, i.e. spring and damper elements. Figure 3.6 shows the 7 DOF torsional vibration model of a four-cylinder four-stroke SI engine-load configuration considered in this thesis. As it is seen, the model is modular and thus it is straightforward to add more cylinders. Here, the four cylinders are assumed to have the same structure. $T_{\mathrm{tot},i}(t)$ is the total engine fluctuating torque acting on each crank-slider mechanism J_i, $i = 2, \ldots, 5$ and it will be calculated in Section 3.2. $T_{\mathrm{load}}(t)$ is the braking dynamometer torque which is available as measurement. It is crucial to note that understanding the entire system behavior demands the modeling of the overall system. Therefore, analyzing the properties of the individual parts is not sufficient since modeling of the coupling effects and the existing dynamic interaction between different components are of great importance.

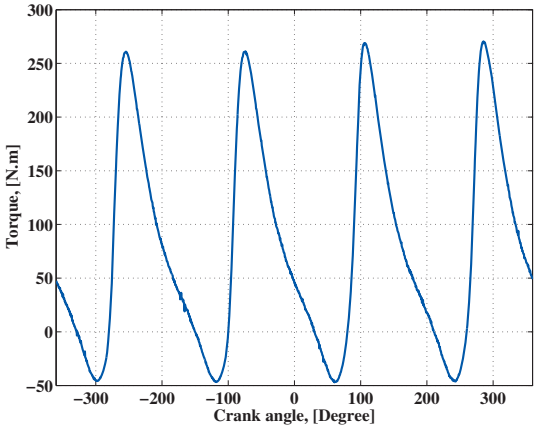

Figure 3.7: *Torque signal of a four-cylinder four-stroke IC engine in two complete rotations of the crankshaft.*

3.2 Engine Excitation

The main source of excitation in an engine-load system is the torque fluctuation due to cyclical operation of the engine, namely two or four-stroke cycles. However, faulty conditions such as late ignition or misfire can also inject serious vibration issues which will be discussed in Chapter 5. Figure 3.7 presents the delivered torque signal of a four-cylinder four-stroke IC engine in two complete rotations of the crankshaft, i.e. 720 degree of the crank angle. As shown, the varying generated torque by the engine is a pulse series where each pulse represents the power stroke of the corresponding cylinder.

This thesis is focused on the torsional vibrations due to the oscillatory engine torque shown in Figure 3.7, although other types of vibrations can also take place. A schematic of the piston crank-slider mechanism is presented in Figure 3.8. In one engine cycle, three different forces act on the connecting rod L which result in a fluctuating torque T applied on each inertia J_i, $i = 2, \ldots, 5$, shown in Figure 3.6. The first is compression pressure force F_{pres} arising from the varying in-cylinder pressure, the second is inertia force F_{inert} due to the inertias of reciprocating masses, and the third is friction force. Frictional forces are due to piston and ring friction losses as well as pumping losses. Considering the engine friction model in Section 3.1.1, the remaining applied friction force on the connecting rod can be assumed to be negligible in comparison to the other two forces. Therefore, the total delivered torque T on the crankshaft is composed of the indicated torque and the reciprocating torque which originate from in-cylinder pressure and inertia effects, respectively.

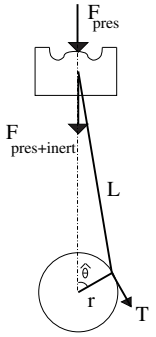

Figure 3.8: *Forces on the crank-slider mechanism.*

3.2.1 Indicated torque

The torque which is produced by in-cylinder pressure is usually called indicated torque and can be computed as following for cylinder i

$$T_{\mathrm{ind},i}(\theta_i^*) = F_{\mathrm{pres},i}(\theta_i^*)\, f(\theta_i^*) r \tag{3.1}$$

where r is crank radius, see Figure 3.8. Moreover $F_{\mathrm{pres},i}$ is the ith compression pressure force and $f(\theta_i^*)$ is the crank-slider mechanism geometric expression which are evaluated as follows, respectively

$$\begin{aligned} F_{\mathrm{pres},i}(\theta_i^*) &= A_{\mathrm{p}}(P_{\mathrm{cyl},i}(\theta_i^*) - P_{\mathrm{crank}}) \\ f(\theta_i^*) &= \sin(\theta_i^*) + \frac{r/L \sin(2\theta_i^*)}{2\sqrt{1-(r/L)^2 \sin^2(\theta_i^*)}} \end{aligned} \tag{3.2}$$

see Rizzoni and Zhang (1994). In (3.2), A_{p} is piston area, L is connecting rod length, $P_{\mathrm{cyl},i}$ is the absolute pressure inside ith cylinder, and P_{crank} is crankcase pressure, see Schagerberg and McKelvey (2003). The angle θ_i^* is the ith cylinder crank angle position that can be defined as $\theta_i^* = \theta - \theta_{\mathrm{TDC},i}$ with θ and $\theta_{\mathrm{TDC},i}$ being crank angle and the ith cylinder Top Dead Center (TDC) crank angle position, respectively. $\theta_{\mathrm{TDC},i}$ depends on the engine firing order and can happen at $\{0°, 180°, 360°, 540°\}$ degrees. Since the calculated torque in (3.1) is for the firing situation of the engine, it is also known as firing indicated torque. Furthermore, if the engine is running without combustion in one of the cylinders, the motoring indicated torque can also be evaluated using (3.1) and (3.2) but $P_{\mathrm{cyl},i}(\theta_i^*)$ should be substituted with $P_{\mathrm{mot,cyl},i}(\theta_i^*)$. Firing and motoring indicated torques are shown in Figure 3.9 for a four-stroke SI engine while the engine is operating at the speed 1200 Revolution Per Minute (RPM) and ~ 57 N.m load.

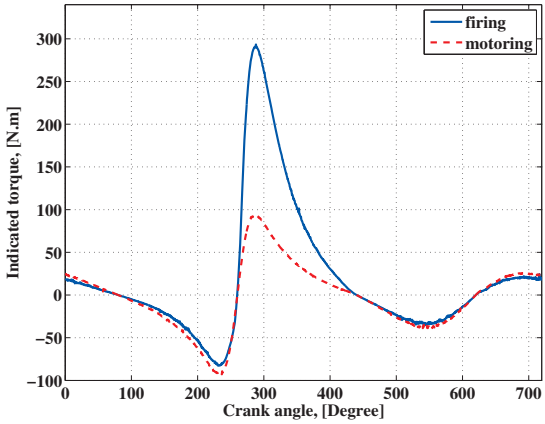

Figure 3.9: *Firing and motoring indicated torques.*

Engine order

The number of excitations which takes place during one revolution of the crankshaft system is important for evaluating the engine orders. For example, a four-stroke IC engine generates one excitation in two crankshaft revolutions. The four strokes are intake, compression, expansion, and exhaust, see Eriksson and Nielsen (2014). Figure 3.10 illustrates the in-cylinder pressure signal for an SI engine where the four strokes are also depicted. The operating point is $<$ 1200 RPM,$\sim$ 57 N.m$>$. The engine orders for the four-stroke cycle are calculated by multiplying the engine speed with factors $1/2, 1, 3/2, 2$, etc. It is important that the natural frequencies of the system do not coincide with any of these orders, at any engine speed, to avoid resonance. An order analysis can be performed to find the amplitude of a specific engine order with respect to engine speed, see Ponti (2008). Therefore, utilizing a sweeping engine speed signal for order analysis can help find the natural frequencies of the system.

3.2.2 Reciprocating torque

The applied torque on the crankshaft due to the inertias of reciprocating masses is called reciprocating torque. The inertia force $F_{\text{inert},i}$ for cylinder i, which has been shown also in Figure 3.8, can be evaluated as follows

$$F_{\text{inert},i}(\theta_i^*) = -m_{\text{eq}} a(\theta_i^*) \tag{3.3}$$

where m_{eq} is the equivalent mass of reciprocating parts and a is the linear acceleration of these components, see Filipi and Assanis (2001),

$$a(\theta_i^*) = r\left[f(\theta_i^*)\ddot{\theta}_i^* + \frac{df(\theta_i^*)}{d\theta_i^*}\dot{\theta}_i^{*2}\right] \tag{3.4}$$

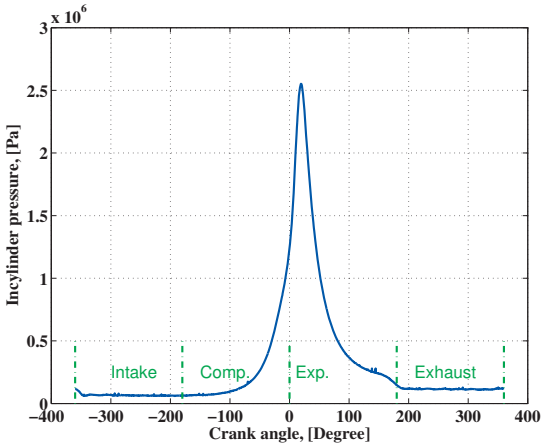

Figure 3.10: *In-cylinder pressure signal for an SI four-stroke engine.*

in which $\dot{\theta}_i^*$ and $\ddot{\theta}_i^*$ are crankshaft angular velocity and acceleration, respectively. Moreover, $f(\theta_i^*)$ has been given in (3.2). As mentioned by Ponti (2008), the first term inside the bracket in (3.4) is negligible in comparison to the other term. Therefore, by using (3.3) and (3.4), the approximate relation for reciprocating torque is

$$T_{\text{recip},i}(\theta_i^*) = -m_{\text{eq}} r \left[\frac{df(\theta_i^*)}{d\theta_i^*} \dot{\theta}_i^{*2} \right] f(\theta_i^*) r. \tag{3.5}$$

3.2.3 Total fluctuating torque

Finally, considering the calculations in Sections 3.2.1 and 3.2.2, the total applied torque on each inertia J_i, $i = 2, \ldots, 5$ which is representing the crank-slider mechanism can be computed, see Figure 3.6. If the crank angle θ in relation $\theta_i^* = \theta - \theta_{\text{TDC},i}$ in (3.1)–(3.5) is measured in time, then the total torque can also be expressed in time as

$$T_{\text{tot},i}(t) = T_{\text{ind},i}(t) + T_{\text{recip},i}(t). \tag{3.6}$$

3.3 Continuous-time mathematical model of the crankshaft

By defining θ_i as the ith inertia angular position in Figure 3.6, the Newton's second law can be used to describe the angular acceleration for each inertia J_i.

Consequently, the model equations of motion can be written as

$$J_i\ddot{\theta}_i = C_{i+1,i}(\dot{\theta}_{i+1} - \dot{\theta}_i) + K_{i+1,i}(\theta_{i+1} - \theta_i)\,, \qquad \text{for } i = 1, \tag{3.7}$$

$$\begin{aligned} J_i\ddot{\theta}_i =& C_{i+1,i}(\dot{\theta}_{i+1} - \dot{\theta}_i) - C_i\dot{\theta}_i \\ &+ K_{i+1,i}(\theta_{i+1} - \theta_i) - C_{i,i-1}(\dot{\theta}_i - \dot{\theta}_{i-1}) \\ &- K_{i,i-1}(\theta_i - \theta_{i-1}) + T_{\text{tot},i}(t)\,, \qquad \text{for } i = 2,\ldots,5, \end{aligned} \tag{3.8}$$

$$\begin{aligned} J_i\ddot{\theta}_i =& C_{i+1,i}(\dot{\theta}_{i+1} - \dot{\theta}_i) + K_{i+1,i}(\theta_{i+1} - \theta_i) \\ &- C_{i,i-1}(\dot{\theta}_i - \dot{\theta}_{i-1}) - K_{i,i-1}(\theta_i - \theta_{i-1})\,, \qquad \text{for } i = 6, \end{aligned} \tag{3.9}$$

$$J_i\ddot{\theta}_i = -C_{i,i-1}(\dot{\theta}_i - \dot{\theta}_{i-1}) - K_{i,i-1}(\theta_i - \theta_{i-1}) - T_{\text{load}}(t)\,, \qquad \text{for } i = 7, \tag{3.10}$$

where, as mentioned in Section 3.1.1, $C_{i,i-1}$ and C_i are viscous damping coefficients and $K_{i,i-1}$ is the stiffness coefficient. Furthermore, $T_{\text{tot},i}(t)$ is given in (3.6).

3.3.1 State-space formulation

For the system identification approach which is to be used in this thesis, i.e. grey-box modeling, the state-space representation of the engine-load system given in Figure 3.6 is required. By introducing $(\theta_i(t) - \theta_{i-1}(t))$ and $\dot{\theta}_i(t)$ in (3.7)-(3.10) as the state variables, the following 13×1 state vector $x(t)$ is defined

$$\begin{aligned} x_{13\times1} =& \big[\dot{\theta}_1, \dot{\theta}_2, \theta_2 - \theta_1, \dot{\theta}_3, \theta_3 - \theta_2, \dot{\theta}_4, \\ & \theta_4 - \theta_3, \dot{\theta}_5, \theta_5 - \theta_4, \dot{\theta}_6, \theta_6 - \theta_5, \dot{\theta}_7, \theta_7 - \theta_6\big]. \end{aligned} \tag{3.11}$$

By looking at the engine torque calculations in (3.1)-(3.5), it is seen that these relations are extremely nonlinear with respect to θ_i^*. This is, as described before, due to the crank-slider mechanism kinematics. If the angular position of each intertia J_i, i.e. θ_i, is used in (3.1)-(3.5) instead of crank angle θ, the state-space equations will be highly nonlinear, see Rizzoni and Zhang (1994). Accordingly, so far, a simplification has been done in which the unknown state θ_i is replaced with the measured crank angle in the computations of indicated and reciprocating torques, see Section 3.2.3. However, due to the squared states $\dot{\theta}_i(t), i = 2,\ldots,5$ in $T_{\text{tot},i}(t)$, the corresponding state-space representation of the engine-load system is still nonlinear and can be written as follows

$$\dot{x}(t) = f(x(t), u(t)) \tag{3.12}$$

where $u(t)$ is the system input vector of size 5×1 consisting of engine and load torques. Now, the second approximation can be considered to remove the nonlinearity by substituting $\dot{\theta}_i^2, i = 2,\ldots,5$ in $T_{\text{tot},i}(t)$ with the square of system

output which is the measured damping wheel angular velocity $x_1(t) = \dot{\theta}_1(t)$. In this way, the input $u(t)$ in (3.12) will be independent of the states and can be calculated separately. The results of the estimated model validation in Chapter 4 imply that these approximations, which are essential to acquire a linear model, will not influence the system output considerably. Therefore, the model is now characterized in the common continuous-time LTI state-space form

$$\begin{aligned} \dot{x}(t) =& A(p)x(t) + B(p)u(t) \\ z(t) =& \dot{\theta}_1(t) = [1\ 0...0]x(t) \end{aligned} \tag{3.13}$$

in which p is the vector of system unknown parameters, i.e. inertias, stiffness, and damping coefficients presented in Figure 3.6, which are to be estimated. The system matrices $A(p)$ and $B(p)$ are given in Appendix A. Since there is a finite number of state variables, the system is lumped and not distributed.

Chapter 4

Engine-load model identification

In this chapter, the PEM described in Section 2.2.2 is used to identify the unknown parameters of an engine-load system torsional vibration model represented by the grey-box structure (3.13). The estimation is based on the PO approach and is done on both real data and simulation data to better illustrate the convergence performance of different parameters. It is shown how the original lumped model of the engine-load system torsional vibration, depicted in Figure 3.6, can be further simplified if the application of interest considers a specific frequency region. Accordingly, first a number of parameters can be obtained using the simplified model and next these estimated parameters can be utilized in the 7 DOF model structure. This reduces the number of unknowns during estimation which improves the performance. Moreover, the importance of the data information for estimating a specific parameter is shown by using two different kinds of data sets. The first data set consists of 10 cycles of normal engine operation and the input is firing indicated torque, while the second data set includes the case in which the combustion is missing for one of the cylinders during 10 cycles. Hence, in the latter case, motoring indicated torque is considered as input and this faulty situation is called *misfire* phenomenon.

All the estimation procedures in this chapter are made using Matlab System Identification Toolbox, `greyest` command specifically, which is based on PEM for parameter estimation of grey-box models, see Ljung (1988-2014).

4.1 Experimental setup

A schematic view of the experimental setup in the engine laboratory at the Division of Vehicular Systems is given in Figure 4.1. It is equipped with a four-cylinder IC spark ignited engine with firing order 1342. The engine is controlled using dSPACE-equipment, with a fully transparent control system

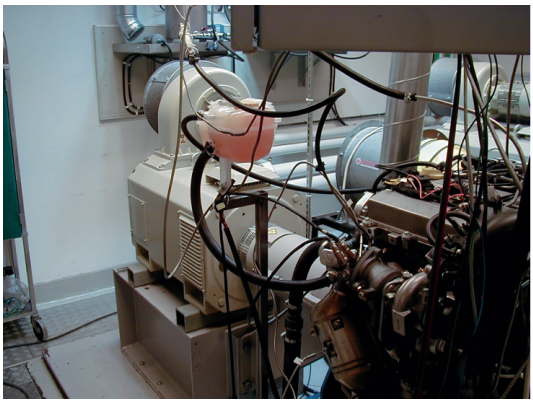

Figure 4.1: *Schematic view of the experimental setup in the engine laboratory at Division of Vehicular Systems, Leufven (2013).*

built in Matlab Simulink and executed in real-time, Leufven (2013). A modern asynchronous machine (dynamometer), which can perform both as a drive and a load to the engine, is also provided. It has a braking capability of 250 kW ($\sim$ 340 hp) and a rated torque of 480 N.m. The dynamometer also acts as start motor for the combustion engine. The sensors of the dynamometer deliver the shaft speed and the applied torque. Moreover, the cylinders 1 and 2 are equipped with in-cylinder pressure sensors and the data acquisition is performed on a crankshaft angle basis. The crank angle sensor measures the time interval between two consecutive teeth with a resolution of 0.5 degree on the damping wheel side. Further, angular velocity measurement which is considered as the system output is generated using these time intervals. The corresponding time vector is also produced which allows doing the identification in time domain.

The data, which is used for the identification approach in this thesis, is collected at the engine operating point $<$ 1200 RPM,$\sim$ 57 N.m$>$ and the sampling frequency of $\sim$ 14402 Hz for both normal and misfire operating conditions.

4.2 Parameter estimation of the simplified 2 DOF model

The identification procedure for the engine-load system starts with estimation of unknown parameters of the simplified model structure given in Figure 4.2. In order to investigate the feasibility of the approach, the estimation is first done using the simulation data from a known system which helps understand the convergence properties of different parameters. The first conclusion from the simulation data analysis, in Section 4.2.1, is that for a good estimation performance the damping coefficient $C_{\text{eng,load}}$, see Figure 4.2, should be fixed. One more result is regarding the data information where it is shown that by

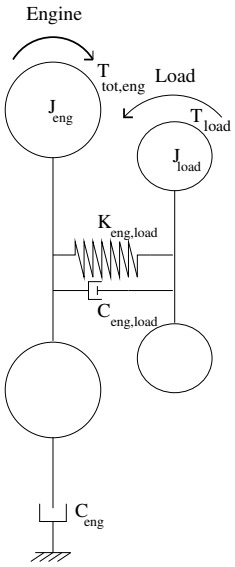

Figure 4.2: *Schematic view of a 2 DOF simplified model structure for the engine-load system.*

using engine normal operating data set, J_{load} does not converge to its true value. However, this problem will be solved by applying the misfire data set, see the results in Table 4.3.

4.2.1 Estimation on simulated data

The inputs of the simplified 2 DOF model which is shown in Figure 4.2 are the total engine torque $T_{\text{tot,eng}}(t)$ and the load torque $T_{\text{load}}(t)$. The total engine torque $T_{\text{tot,eng}}(t)$ is generated by summing up the torques $T_{\text{tot},i}(t)$ given in (3.6), for $i = 2, \ldots, 5$. As seen in (3.5), $T_{\text{tot},i}(t)$ is nonlinearly related to the state $\dot{\theta}_{\text{eng}}(t)$ which is the system output and is measured. This is due to the reciprocating torque relation. In order to have a linear state-space equation for the model of the engine-load system, the engine input torque can be calculated before the estimation by substituting the measured angular velocity in (3.5). To illustrate that this assumption will not influence the results, the crankshaft angular velocity signal $\dot{\theta}_{\text{eng}}(t)$ is produced by simulating the known nonlinear state-space system (4.1) and then the simulated output is used besides a linear

model structure to estimate the desired parameters.

$$\begin{aligned}
\dot{x}_1(t) =& \frac{1}{J_{\text{eng}}}\big(- C_{\text{eng}}\, x_1(t) + K_{\text{eng,load}}\, x_3(t) + \\
& C_{\text{eng,load}}\,(-x_1(t) + x_2(t)) + T_{\text{tot,ind}}(t) + x_1^2(t)\, T^*_{\text{tot,recip}}(t)\big) \\
\dot{x}_2(t) =& \frac{1}{J_{\text{load}}}\big(- K_{\text{eng,load}}\, x_3(t) - C_{\text{eng,load}}\,(-x_1(t) + x_2(t)) - T_{\text{load}}(t)\big) \\
\dot{x}_3(t) =& x_2(t) - x_1(t) \\
\text{Output} : & \; y(t) = x_1(t) + e(t).
\end{aligned} \tag{4.1}$$

In (4.1), $x(t) = [\dot{\theta}_{\text{eng}}(t) \;\; \dot{\theta}_{\text{load}}(t) \;\; \theta_{\text{eng}}(t) - \theta_{\text{load}}(t)]^{\text{T}}$ is the state vector and $\dot{\theta}_{\text{eng}}(t)$ is the model output. The physical parameters $1/J_{\text{eng}}$, $C_{\text{eng,load}}$, $K_{\text{eng,load}}$, C_{eng}, and $1/J_{\text{load}}$ are to be estimated. The true values of these parameters are acquired from the results in Section 4.2.2 and are given in Table 4.1. It is assumed that the measurement noise $e(t)$ is white with zero mean and standard deviation 0.1 rad/sec. $T_{\text{tot,ind}}(t)$ and $T^*_{\text{tot,recip}}(t)$ are computed as follows

$$\begin{aligned}
T_{\text{tot,ind}}(t) &= \sum_{i=2}^{5} T_{\text{ind},i}(t) \\
T^*_{\text{tot,recip}}(t) &= \sum_{i=2}^{5} T^*_{\text{recip},i}(t)
\end{aligned} \tag{4.2}$$

where $T_{\text{ind},i}(t)$ is given in (3.1) and $T^*_{\text{recip},i}(t)$ is calculated using (3.5) excluding $\dot{\theta}_i^{*2}$. The other parameters that are used in (3.1)-(3.5) are geometric properties of the current engine, i.e. r, L, A_p, and the equivalent mass of the reciprocating parts m_{eq} which is assumed to be known. These are given in Table 4.2.

Table 4.1: *True parameters for continuous-time model structure given in (4.1). For description of parameters see Figure 4.2. The values are obtained from the results of estimation on real data, see Section 4.2.2.*

$\frac{1}{J_{\text{eng}}}$	$C_{\text{eng,load}}$	$K_{\text{eng,load}}$	C_{eng}	$\frac{1}{J_{\text{load}}}$
2.557	2.5	1992	0.1541	5.646

Table 4.2: *Known characteristics of the engine.*

r	L	A_p	m_{eq}
0.043	0.145	0.0058	0.7

Now, to identify the parameters of the model (4.1), given in Table 4.1, the

following linear continuous-time state-space model structure $\mathbb{M}_{\text{eng}}$ is used

$$\begin{aligned} \dot{x}(t) &= Ax(t) + Bu(t) \\ y(t) &= x_1(t) + e(t). \end{aligned} \tag{4.3}$$

The state vector and the output of (4.3) are similar as the nonlinear version (4.1), however in this case the input vector is defined as

$$u(t) = [T_{\text{tot,eng}}(t) \;\; T_{\text{load}}(t)]^{\text{T}} \tag{4.4}$$

where, as described earlier, the total engine torque $T_{\text{tot,eng}}(t)$ is found by summing up the torques $T_{\text{tot},i}(t)$ given in (3.6), for $i = 2, \ldots, 5$, having in-cylinder pressure $P_{\text{cyl},i}(t)$. Furthermore, the term $x_1^2(t)$ in (4.1) is substituted with the crankshaft angular velocity $\dot{\theta}_{\text{eng}}(t)$ which is the simulated output of (4.1). Accordingly the nonlinear term disappears and will be inside $T_{\text{tot,eng}}(t)$. Since the estimation is done on the simulated data from a known system, the process noise $w(t)$ will be zero and thus in the innovation form (2.10), the feedback terms are zero. Accordingly, the system matrices in (4.3) and its corresponding innovation form are as follows

$$\begin{aligned} A &= \begin{bmatrix} -\frac{1}{J_{\text{eng}}}(C_{\text{eng,load}} + C_{\text{eng}}) & \frac{1}{J_{\text{eng}}}C_{\text{eng,load}} & \frac{1}{J_{\text{eng}}}K_{\text{eng,load}} \\ \frac{1}{J_{\text{load}}}C_{\text{eng,load}} & -\frac{1}{J_{\text{load}}}C_{\text{eng,load}} & -\frac{1}{J_{\text{load}}}K_{\text{eng,load}} \\ -1 & 1 & 0 \end{bmatrix} \\ B &= \begin{bmatrix} \frac{1}{J_{\text{eng}}} & 0 \\ 0 & -\frac{1}{J_{\text{load}}} \\ 0 & 0 \end{bmatrix}. \end{aligned} \tag{4.5}$$

Since we have sensors available only for cylinders 1 and 2, in-cylinder pressures 3 and 4 are assumed to be the same as the other two cylinders. However, in order to keep the corresponding firing order 1342, the signals have to be shifted. The pressures are shown in Figure 4.3 for two engine cycles.

The braking torque $T_{\text{load}}(t)$ in (4.4) is representing the load which is due to the road and aerodynamic forces when the engine is placed on-board a car. The measured $T_{\text{load}}(t)$ is given in Figure 4.4. It is exposed to high-frequency disturbances which should be prefiltered. Therefore, the measured braking torque signal is smoothed further by using a moving average filter. The resulted smoothed version is also demonstrated in Figure 4.4 which is approximately constant during the experiment time. Finally, an example of the input and simulated output data sets, which are to be applied in the identification approach of this section, are shown in Figure 4.5. Both normal combustion and misfire cases are given where misfire occurs in cylinder 2. $T_{\text{load}}(t)$ has been smoothed and a white measurement noise $e(t)$ with zero mean and standard deviation 0.1 rad/sec has been added to the simulated outputs.

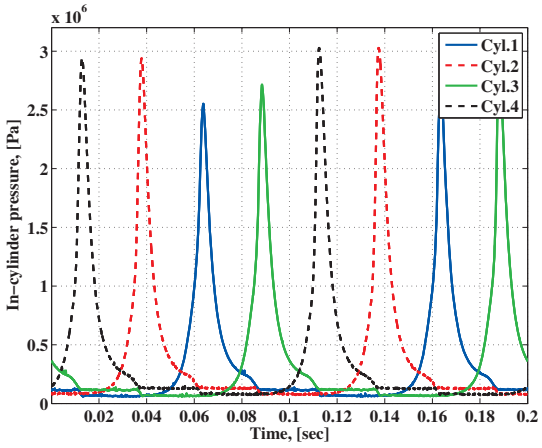

Figure 4.3: *In-cylinder pressure signals, Cyl.*1 *and Cyl.*2 *are measured while Cyl.*3 *and Cyl.*4 *are constructed by shifting according to the firing order* 1342*. The operating point is* $<$ 1200 *RPM,*$\sim$ 57 *N.m*$>$*.*

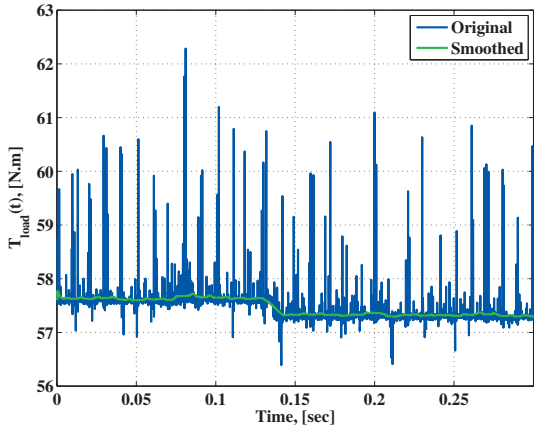

Figure 4.4: *The measured* $T_{load}(t)$ *before and after smoothing.*

Problem statement

The parameters of the model structure $\mathbb{M}_{\text{eng}}$ presented in (4.3) have been given in Table 4.1. They are denoted by the parameter vector p_{eng} and it is assumed that all the 5 parameters are unknown and to be estimated. To avoid nonlinearity in parameters, as much as possible, the inverse of J_{eng} and J_{load} are estimated. The normal combustion and the misfire data sets have 14400 samples with a sampling frequency of 14402 Hz.

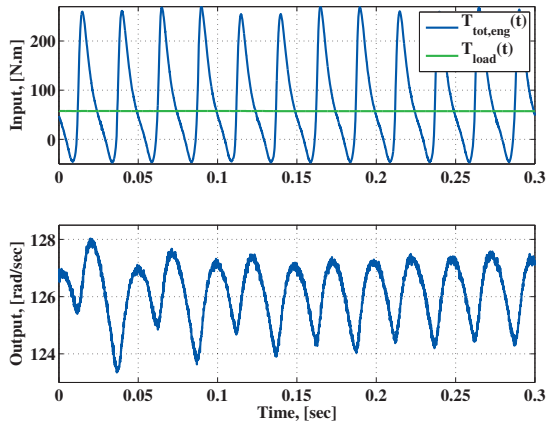

(a) *Normal combustion data set.*

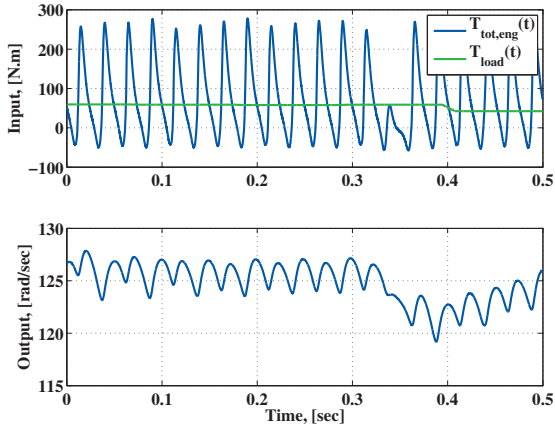

(b) *Misfire data set.*

Figure 4.5: *Example of input and simulated output data sets used for identification, Operating point* $<$ 1200 *RPM,*$\sim$ 57 *N.m*$>$*. Three engine cycles have been plotted here.*

According to Section 2.2.2, before starting any estimation approach it is reasonable to investigate the structural identifiability of the model $\mathbb{M}_{\text{eng}}$, see the Definitions 2.*a*–2.*c* in Chapter 2. Here the symbolic approach, i.e. the repeated Lie-derivative calculations, is illustrated and used to obtain the extended observability matrix $\mathbb{O}(x, p, u_1, \ldots, u_m^{(\kappa-1)})$ given in (2.29) for the 2 DOF model (4.3). For the sake of simplicity, it is assumed that only one parameter is unknown: J_{eng}. Moreover, for notational simplicity, $\alpha = \frac{1}{J_{\text{eng}}}$ is defined and the other remaining four parameters, i.e. J_{load}, $C_{\text{eng,load}}$, $K_{\text{eng,load}}$, and C_{eng}, are set to 1. Considering $y = \eta(x, p) = x_1(t)$ and the input $u(t)$ given in (4.4), the matrix $\mathbb{O}$

for this case is found as follows

$$\mathbb{O} = \begin{bmatrix} \frac{\partial \eta(x,p)}{\partial x_1} & \frac{\partial \eta(x,p)}{\partial x_2} & \frac{\partial \eta(x,p)}{\partial x_3} & \frac{\partial \eta(x,p)}{\partial \alpha} \\ \vdots & \vdots & \vdots & \vdots \\ \frac{\partial \eta^{(3)}(x,p)}{\partial x_1} & \frac{\partial \eta^{(3)}(x,p)}{\partial x_2} & \frac{\partial \eta^{(3)}(x,p)}{\partial x_3} & \frac{\partial \eta^{(3)}(x,p)}{\partial \alpha} \end{bmatrix} = \begin{bmatrix} \mathbb{O}_{x_1} & \mathbb{O}_{x_2} & \mathbb{O}_{x_3} & \mathbb{O}_{\alpha} \end{bmatrix} \tag{4.6}$$

where the corresponding columns are

$$\mathbb{O}_{x_1} = \begin{bmatrix} 1 \\ -2\alpha \\ 4\alpha^2 \\ \alpha - 8\alpha^3 \end{bmatrix} \mathbb{O}_{x_2} = \begin{bmatrix} 0 \\ \alpha \\ -2\alpha^2 \\ -\alpha + 4\alpha^3 \end{bmatrix} \mathbb{O}_{x_3} = \begin{bmatrix} 0 \\ \alpha \\ -\alpha - 2\alpha^2 \\ 2\alpha^2 + 4\alpha^3 \end{bmatrix} \tag{4.7}$$

$$\mathbb{O}_{\alpha} = \begin{bmatrix} 0 \\ X_1 + U_1(0, 0, T_{\text{tot,eng}}) \\ -x_3 - 4\alpha X_1 + U_1(0, T_{\text{tot,eng}}, \dot{T}_{\text{tot,eng}}) - T_{\text{load}} \\ (-1 - 4\alpha)X_3 - 4\alpha(-T_{\text{load}} + X_2) + 12\alpha^2 X_1 + U_1(T_{\text{tot,eng}}, \dot{T}_{\text{tot,eng}}, \ddot{T}_{\text{tot,eng}}) - \dot{T}_{\text{load}} \end{bmatrix}$$

where $X_1 = -2x_1 + x_2 + x_3$, $X_2 = x_1 - x_2 - x_3$, $X_3 = x_2 - x_1$ and

$$U_1(u_1, u_2, u_3) = 12\alpha^2 u_1 - 4\alpha u_2 + u_3. \tag{4.8}$$

Assuming that the input vector $u(t)$ is informative enough, the maximum rank for matrix $\mathbb{O}$ in (4.6) is 4 for almost all values of the states x and thus the parameter $\alpha = \frac{1}{J_{\text{eng}}}$ is identifiable. Doing the same calculations for the 2 DOF model (4.3) with five unknown parameters gives the maximum rank of the extended observability matrix equal to 8 which also proves that all the five model unknown parameters are identifiable.

The estimation is first done on noise-free data and the true values of the parameters are used as initial guesses. This is to see if it is possible at all to converge to the true values of the parameters. Then, the estimation is done on noisy data while simultaneously the parameters initial guesses have some offset compared to the true values. The estimated covariance matrix is a suitable tool to see the importance of different parameters for describing the model output using the current data set. A small value of the ith diagonal element of the covariance matrix indicates that the ith model parameter has significant influence on the system response for this specific model structure and data set. In other words, the current input is informative enough for estimating the mentioned parameter. It is shown that the results of the identification are promising when misfire data set is used as estimation data. This also validates the assumption of applying a linear model structure (4.3) instead of the original nonlinear state-space system (4.1), see also Section 3.3.1.

Table 4.3: *Estimated and real value of the parameter vector p_{eng} for continuous-time model (4.3). All the 5 parameters are estimated together by using noise-free data and true values as initial guesses, Estimation data at operating point <1200 RPM,~ 57 N.m$>$.*

(a) *Normal combustion data set.*

	True	Estimated	Covariance ($\times 10^{-6}$)	Error%
$\frac{1}{J_{\text{eng}}}$	2.557	2.732	6	6.84
$C_{\text{eng,load}}$	2.5	3.503	1815	40.12
$K_{\text{eng,load}}$	1992	836	106	58
C_{eng}	0.1541	0.1541	0	0
$\frac{1}{J_{\text{load}}}$	5.646	20.14	84118	256

(b) *Misfire data set.*

	True	Estimated	Covariance ($\times 10^{-6}$)	Error%
$\frac{1}{J_{\text{eng}}}$	2.557	2.551	4.39	0.24
$C_{\text{eng,load}}$	2.5	3.887	613	55.48
$K_{\text{eng,load}}$	1992	2122	18	6.53
C_{eng}	0.1541	0.1535	0	0.39
$\frac{1}{J_{\text{load}}}$	5.646	5.427	208	3.88

Noise-free simulation and true initial parameter vector

The true parameters of the continuous-time state-space model (4.3) are used as the initial guesses for unknown parameters to be identified and are shown in Table 4.3(a). The estimated values are also shown together with the corresponding estimated covariances. The data set which contains the normal operating condition <1200 RPM,~ 57 N.m$>$ is applied for estimation. According to Table 4.3(a), the largest estimated covariance as well as the biggest error is obtained for the inverse of load inertia $1/J_{\text{load}}$. This implies that the output of the estimated model $\mathfrak{m}_{\text{eng}}$, which is the crankshaft angular velocity $\dot{\theta}_{\text{eng}}(t)$, is not significantly affected by this parameter. In other words, there is not enough information for estimation of the load inertia in the current data set using the current model structure. However, applying the data set from misfire operating condition will solve this issue as it is shown in Table 4.3(b) where the results of using this new data set are given. As it is seen, there is a considerable decrease in the values of estimated covariances and the errors, whereas damping coefficient $C_{\text{eng,load}}$ does not still converge to its true value.

To see the convergence performance of all the 5 parameters given in Table 4.1, for each parameter $p_{\text{eng},i}$, $i = 1...5$, the interval $[0\,,\, 2.5\,p_{\text{eng},i}]$ is divided into a number of points. Then the loss function $V_N(p, Z^N)$, see (2.16), is determined for all these points within the mentioned interval. One parameter at a time

is changed while the other parameters are fixed. The results are shown in Figure 4.6. A U-shape loss function with a minimum at the parameter true value is expected. However, as shown in Figures 4.6(a)-(b), the loss function is U-shape only for 2 out of 5 parameters: $1/J_{\text{eng}}$ and C_{eng}. These 2 parameters have also the smallest estimated covariances in Table 4.3(b). The loss functions of the remaining 3 parameters are not U-shape and are shown in logarithm scale in order to be more illustrative. As it is seen in Figure 4.6(e), for damping coefficient $C_{\text{eng,load}}$ there exists no minimum in the function which is the reason for difficulty in estimation of this parameter and it causes the biggest error and largest estimated covariance in Table 4.3(b).

Having the above discussion, it is reasonable to fix the damping coefficient to an appropriate value and skip estimating this parameter. The estimation results and the model fit to the validation data are shown in Table 4.4 and Figure 4.7, respectively. In this case the damping coefficient $C_{\text{eng,load}}$ is fixed during identification. Model fit is determined by using (2.32) in which the model simulated output $\hat{y}_s(t|\mathfrak{m}_{\text{eng}})$ is considered, see Section 2.2.3 and relation (2.31) for more information. Since misfire data set has been used already for estimation, the normal combustion data set is used for validation. A good model fit besides low estimation covariances and errors are signs of reliable estimation.

Table 4.4: *Estimated and real value of the parameter vector p_{eng} for continuous-time model (4.3). Damping coefficient $C_{eng,load} = 2.5$ is fixed and the other 4 parameters are estimated together by using noise-free data and true values as initial guesses, Estimation data is misfire input/output at operating condition <1200 RPM,~ 57 N.m>.*

	True	Estimated	Covariance ($\times 10^{-6}$)	Error%
$\frac{1}{J_{\text{eng}}}$	2.557	2.497	4.7	2.35
$K_{\text{eng,load}}$	1992	1978	15.4	0.70
C_{eng}	0.1541	0.1536	0	0.32
$\frac{1}{J_{\text{load}}}$	5.646	6.014	247	6.5
fit(%)	61			

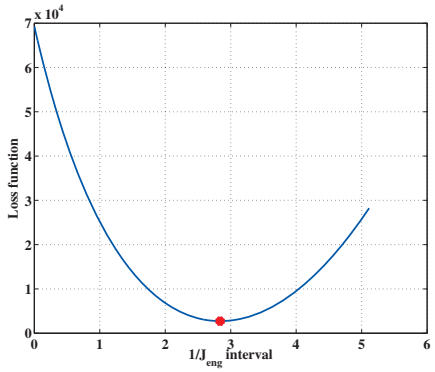

(a) *Engine inertia inverse,* $\frac{1}{J_{eng}}$

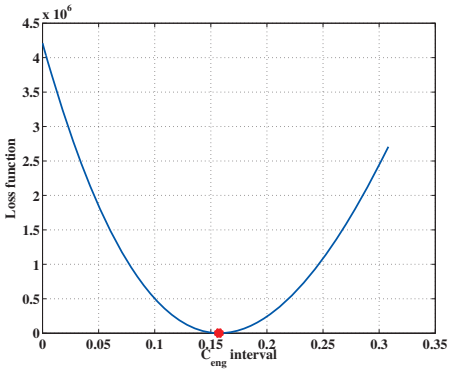

(b) *Friction,* C_{eng}

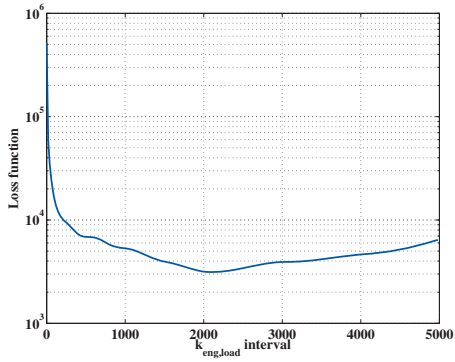

(c) *Stiffness,* $K_{eng,load}$

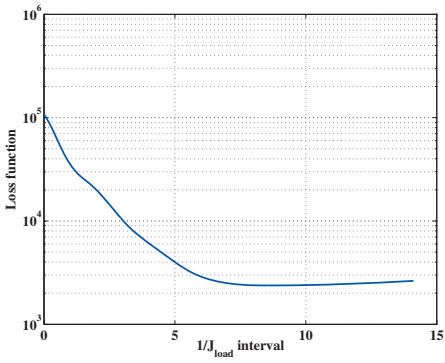

(d) *Load inertia inverse,* $\frac{1}{J_{load}}$

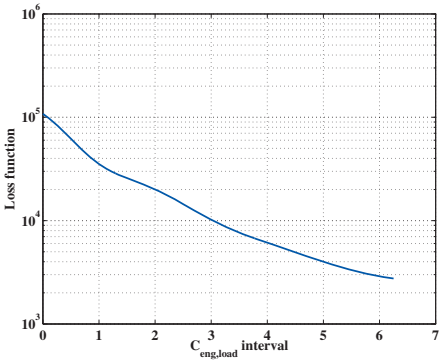

(e) *Damping,* $C_{eng,load}$

Figure 4.6: *Loss function* $V_N(p, Z^N)$ *value at different points in the interval* $[0\,,\,2.5\,p_{eng,i}]$, $i = 1...5$. *For each case one parameter* $p_{eng,i}$ *is changing while the others are fixed.*

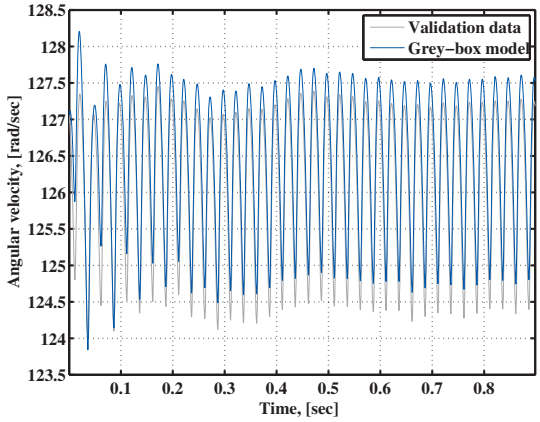

Figure 4.7: *True output signal (gray) and simulated output (blue) from the estimated grey-box model* $\mathfrak{m}_{eng}$ *for simulated validation data, noise-free data and true values as initial guesses.*

Noisy simulation and initial parameter vector offset

In this case, a white measurement noise $e(t)$ with zero mean and standard deviation 0.1 rad/sec is added to the simulated output, see (4.1). Hence, it can be studied how much the noisy data will influence the identification performance. Furthermore, it is improbable that the initial guesses of the parameters will be exactly the true ones, even if a lot of work has been done prior to the estimation. Thus, in order to see whether the estimation approach is robust against wrong initial values, the 10% offset is added to the true parameters and these will be applied as initial guesses. The estimation results and the model fit to the validation data are shown in Table 4.5 and Figure 4.8, respectively. In comparison to the results given in Table 4.4 and Figure 4.7, still the estimated covariances and the corresponding parameter estimation errors are considerably small and the fit value does not deviate. If the estimation begins at initial guesses with (−10% offset), the results are fairly similar to those of Table 4.5 in which the approach initializes at (+10% offset).

4.2.2 Estimation on real data

In this section, the simplified 2 DOF engine-load model, which is depicted in Figure 4.2, is identified by using the *measured* input and output data set. The applied linear model structure $\mathbb{M}_{\text{eng}}$ is similar to the one that is given in (4.3). However, a minor correction should be performed as follows

$$\begin{aligned} \dot{x}(t) &= A(p)x(t) + B(p)u(t) + K(p)e(t) \\ y(t) &= x_1(t) + e(t). \end{aligned} \tag{4.9}$$

Table 4.5: *Estimated and real value of the parameter vector p_{eng} for continuous-time model (4.3). Damping coefficient $C_{eng,load} = 2.5$ is fixed and the other 4 parameters are estimated together by using noisy data and wrong values as initial guesses, Estimation data is misfire input/output at operating condition < 1200 RPM,~ 57 N.m>.*

	True	Initial guess (+10% offset)	Estimated	Covariance ($\times 10^{-6}$)	Error%
$\frac{1}{J_{\text{eng}}}$	2.557	2.8127	2.496	6.6	2.38
$K_{\text{eng,load}}$	1992	2191	1969	21.7	1.15
C_{eng}	0.1541	0.1695	0.1537	0	0.26
$\frac{1}{J_{\text{load}}}$	5.646	6.22	6.059	355	7.32
fit(%)	71.62				

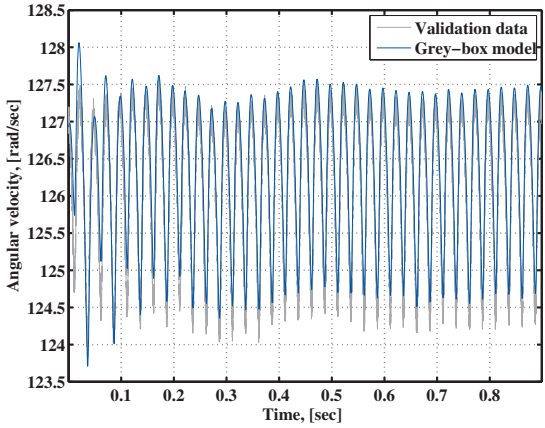

Figure 4.8: *True output signal (gray) and simulated output (blue) from the estimated grey-box model $\mathfrak{m}_{eng}$ for simulated validation data, noisy data and wronge values as initial guesses.*

Since the estimation is done using real data and not the simulated output from a known system, the process noise is present. Therefore, in the innovation form (2.10) and consequently (4.9), the feedback terms $K(p)$ are not zero and are estimated simultaneously with the model physical parameters, i.e. PO approach. The system matrices are given in (4.5).

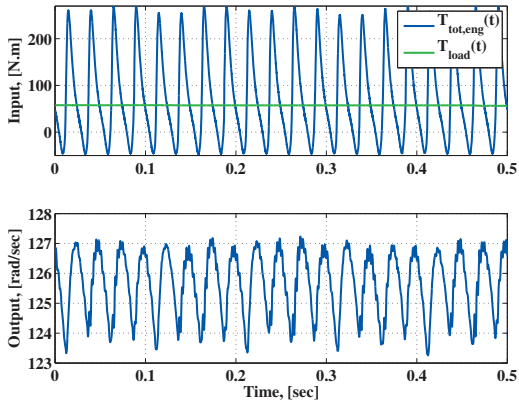

(a) *Normal combustion data set.*

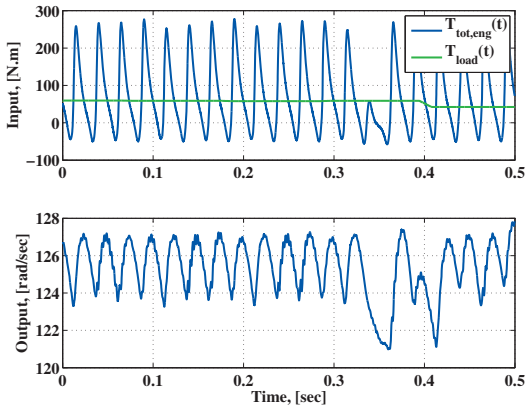

(b) *Misfire data set.*

Figure 4.9: *Example of measured input and output data sets used for identification, Operating point* $<$ 1200 *RPM,*$\sim$ 57 *N.m*$>$*. Four engine cycles have been plotted here.*

The measurements are collected at the engine laboratory of Vehicular Systems Division. As mentioned before, the engine operating point is $<$ 1200 RPM,$\sim$ 57 N.m$>$ while both the speed and load are kept constant. Moreover, the sampling frequency is $\sim$ 14402 Hz and each data set has 14400 samples which is 10 working cycles of the engine. Based on the results of Section 4.2.1, the misfire data set is used for estimation and the estimated model is validated against the normal combustion data set. Furthermore, the damping coefficient is kept constant, $C_{\text{eng,load}} = 2.5$, which is the value obtained from literature, see for example Rabeih (1997); Ponti (2008). Figure 4.9 shows the measured input and output data sets for the model structure given in (4.9) which are to be applied in the identification approach of this section. Both cases of normal

combustion and misfire occurrence are depicted. The braking torque has been already smoothed in Section 4.2.1 to avoid undesired high-frequency noises. Moreover, the given damping wheel angular velocity, as the system output in Figure 4.9, has been also low-pass filtered to reject high-frequency fluctuations. This should be done before running estimation on measured data to increase the identification accuracy by removing the unmodeled dynamics effects. To prevent phase shifts during filtering, `filtfilt` command in Matlab is used which provides zero-phase digital filtering. Figure 4.10 gives the measured damping wheel angular velocity before and after filtering.

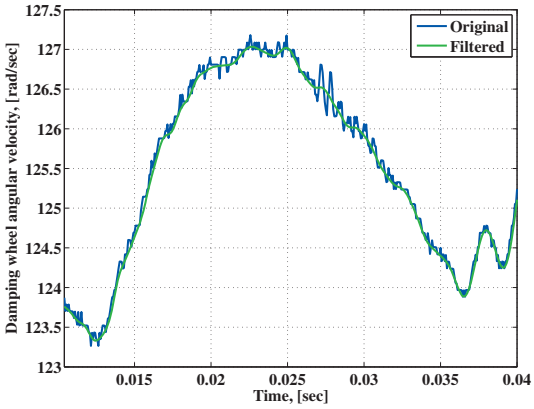

Figure 4.10: *Measured damping wheel angular velocity before and after low-pass filtering, a part of the engine working cycle has been plotted.*

When the measured data set is used, the true values of the system parameters are not known. Consequently the estimated model, denoted by $\mathfrak{m}_{\text{eng},r}$ in which r stands for real data, is validated against validation data where the residual analysis is also a tool to assess the model quality. However, having some extra characteristics of the real system will help to get a better assessment. In modeling of the engine-load system torsional vibrations, the natural frequency of the actual system is one evaluation criterion. It can be obtained by performing an order analysis on the measured damping wheel angular velocity. Engine orders have already been introduced in Chapter 3, Section 3.2.1. Here we look at the 1st engine order amplitude at different speeds to see if there is an unusual increase of amplitude in a specific speed. This indicates that a resonance has occurred at that speed and therefore the system natural frequency can be determined. The damping wheel angular velocity measurements are available at $1000, 1200, 1400, 1800$, and 2000 RPM. By performing Fast Fourier Transform (FFT) on the velocity signals, the first engine order amplitude at each speed is obtained and given in Table 4.6. It seems that the system has a peak (resonance) at 1200 RPM$=20$ Hz. Therefore, the simplified model structure $\mathbb{M}_{\text{eng}}$ given in (4.9) should also have a natural frequency at this value.

Results

The estimation is first done on the original measured misfire data set with sampling frequency $\sim$ 14402 Hz. As described before, one common model validation method is to study the residuals which are the parts of the output data that cannot be explained by the model, see Section 2.2.3. Whiteness and cross-correlation tests are two known techniques to investigate the correlation between output residuals and the cross-correlation between the residuals and the input, respectively. For a model of high quality, correlations are small and within the 99% confidence interval. Figure 4.11 shows the residual test on the validation data set which is the normal combustion data set with sampling frequency $\sim$ 14402 Hz. The whiteness test, i.e. upper plot in Figure 4.11, shows high correlation, and therefore the model is of low quality. A low quality model and poor parameter estimations can be due to small sampling time. The possible reason is unnecessary information in a data set, with high sampling rate, which is to be used for a simplified model structure like the 2 DOF system. Thus the data set is resampled with two different factors of 10 and 20 and the results are given in Figures 4.12 and 4.13, respectively. The correlations between the residuals, i.e. upper plot, have decreased in Figure 4.12 while the cross correlations between the input load torque and the output are still not within the 99% confidence interval. However, this is not the case in Figure 4.13 where all the three different correlations are in the desired range. Therefore, a down-sampling factor 20 is selected for the measurement signals for estimating $\mathfrak{m}_{\text{eng},r}$ using a grey-box model structure $\mathbb{M}_{\text{eng}}$. The results of estimation are given in Table 4.7 including the fit percentage, the estimated parameter values, and their estimation covariances. As can be seen, the covariances are fairly low which indicates the current parameters importance in the model output.

Table 4.6: 1*st engine order amplitudes.*

Engine speed (RPM)	1000	1200	1400	1600	1800	2000
Amplitude (RPM)	0.2693	0.8682	0.6811	0.5364	0.3629	0.3581

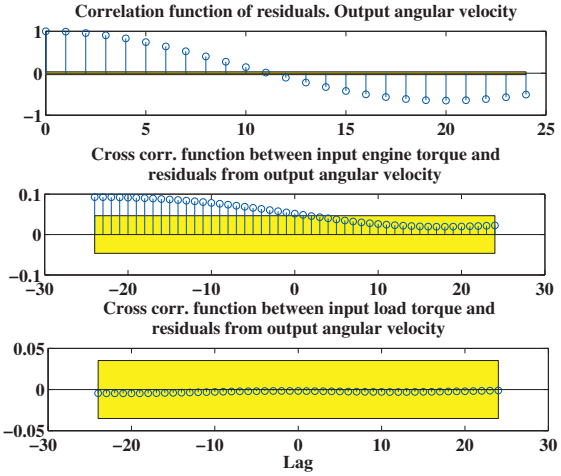

Figure 4.11: *Residual analysis of model structure* $\mathbb{M}_{eng}$ *given in (4.9) using the validation data set with sampling frequency* ~ 14402 *Hz.*

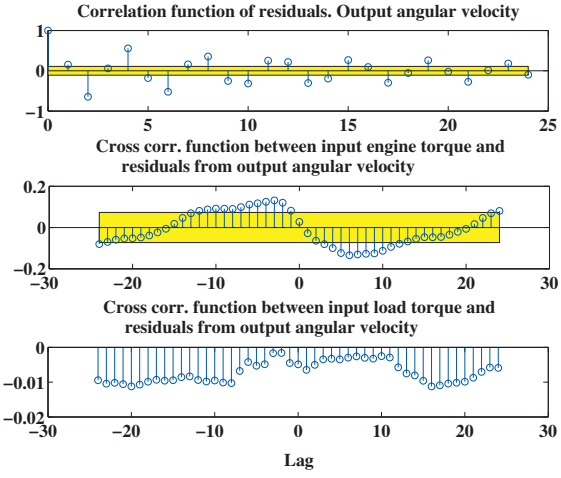

Figure 4.12: *Residual analysis of model structure* $\mathbb{M}_{eng}$ *given in (4.9) using the resampled validation data set with sampling frequency* $\sim 14402/10 = 1440.2$ *Hz.*

Fit to validation data has been plotted and is depicted in Figure 4.14. It is calculated using (2.32) in which the model simulated output $\hat{y}_s(t|\mathfrak{m}_{\text{eng},r})$ is considered. As it is seen, the model output can follow the measured angular velocity and the offsets are not significant, i.e. within ± 1 rad/sec. To illustrate this better, the amplitudes of the main engine frequency and its next two multiples are obtained and given in Table 4.8 for the true and the simulated

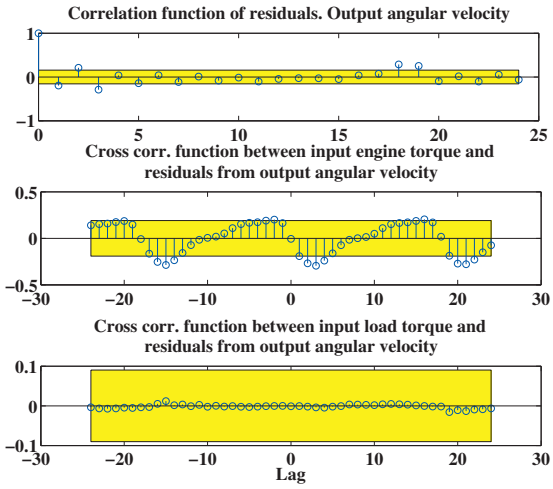

Figure 4.13: *Residual analysis of model structure* $\mathbb{M}_{eng}$ *given in (4.9) using the resampled validation data set with sampling frequency* $\sim 14402/20 = 720.2$ *Hz.*

Table 4.7: *Estimated parameters for continuous-time model (4.9). Estimation data is resampled misfire input/output at operating condition* < 1200 *RPM,*$\sim$ 57 *N.m*$>$ *with sampling frequency* $\sim 14402/20 = 720.2$ *Hz.*

	Estimated	Covariance ($\times 10^{-3}$)
$\frac{1}{J_{\text{eng}}}$	2.557	9.9
$K_{\text{eng,load}}$	1992	127
C_{eng}	0.1541	0.2
$\frac{1}{J_{\text{load}}}$	5.646	13
fit(%)	63.32	

signals. The main engine frequency itself can be calculated as follows

$$f_{\text{main}} = \frac{N\, n_{\text{cyl}}}{60\, n_{\text{ext}}} \tag{4.10}$$

where N is the engine velocity in RPM, here 1200 RPM, n_{cyl} is the number of cylinders, here 4, and n_{ext} is the number of crankshaft revolutions in which one excitation happens, here 2 for the four-stroke SI engine. Accordingly in this case f_{main} is also the 2nd engine order, (see Section 3.2.1 for the definition of engine order). A relatively high fit value besides low correlations in the residual analysis for validation data, see Figure 4.13, prove the estimated model reliability. These results are also a validation for the two assumptions, which were described in Chapter 3, in order to construct a linear model, see Section 3.3.1.

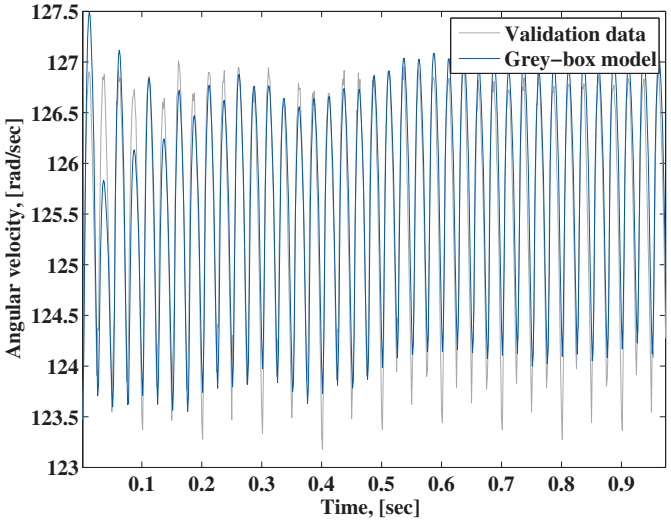

Figure 4.14: *True output signal (gray) and simulated output (blue) from the estimated grey-box model* $\mathfrak{m}_{eng,r}$ *for measured validation data, sampling frequency* $\sim 14402/20 = 720.2$ *Hz.*

Table 4.8: *The amplitudes of the main engine frequency and its two multiples for simulated output from the estimated grey-box model* $\mathfrak{m}_{eng,r}$ *and the true signal, operating point* $<$ 1200 *RPM,*$\sim$ 57 *N.m*$>$*.*

Frequency (Hz)	$f_{\text{main}} = 40$ Hz	$2f_{\text{main}} = 80$ Hz	$3f_{\text{main}} = 120$ Hz
Amplitude (Estimated) (RPM)	6.36	1.47	0.42
Amplitude (True) (RPM)	6.92	1.47	0.5

As a final evaluation, we need to show that the actual system and the model natural frequencies agree with each other. By solving a standard eigenvalue problem, the natural frequencies ω_i of the estimated model $\mathfrak{m}_{\text{eng},r}$ can be written as

$$\omega_i = \sqrt{(\text{Real}(\lambda_i))^2 + (\text{Imag}(\lambda_i))^2} \tag{4.11}$$

where λ_i is the estimated model eigenvalue. Using (4.11), $f_{\lambda_1} = 0.04$ Hz and $f_{\lambda_2} = 20.34$ Hz are obtained. The first natural frequency is approximately zero which is called the rigid body mode. It implies that the angular deformation between the two inertias, J_{eng} and J_{load}, will remain constant at this mode, see Liu and Huston (2011). The second natural frequency coincides with the one that has already been given using the information in Table 4.6 for real data.

It will be illustrated later in Section 4.3.3 that the 2 DOF simplified model is sufficient if the application of interest is in frequency range below 300 Hz.

A note on the value of damping coefficient $C_{\text{eng,load}}$

As described in the optimization results of Section 4.2.1, estimation of the damping coefficient is difficult using the current model structure $\mathbb{M}_{\text{eng}}$ and the current measurements. Therefore, $C_{\text{eng,load}} = 2.5$ is fixed during identification where this value has been found in literature, see Rabeih (1997); Ponti (2008). However, there is one assessment criterion that can be applied to validate this assumption: the amplitude of first engine order in the measured damping wheel angular velocity. Table 4.9 shows the true and the model amplitudes for different values of damping coefficient which helps determine a reasonable value for this parameter. The validation data set, i.e. normal combustion condition, is used in this section.

Table 4.9: *The true and the modeled first engine order amplitudes of damping wheel angular velocity for different damping coefficient $C_{eng,load}$ values.*

	True	Model $C_{\text{eng,load}} = 2.5$	Model $C_{\text{eng,load}} = 2$	Model $C_{\text{eng,load}} = 1.5$
Amplitude (RPM)	0.8682	0.5758	0.7119	0.9258

It is also interesting to perform a Monte Carlo simulation study to obtain the effects of changing a specific parameter, which there exists an uncertainty about, on the system output. Here the damping coefficient $C_{\text{eng,load}}$ is considered to be a random variable with a known uniform distribution in the interval $[1, 10]$. The model $\mathfrak{m}_{\text{eng},r}$ is simulated 1000 times in which the damping coefficient is randomly selected in the mentioned interval. The results of simulations are given in Figure 4.15 and Table 4.10 where the variation in the amplitudes of first engine order and the main frequency, as two important characteristics of damping wheel angular velocity, are analyzed. As it is shown in Table 4.10, the mean values of amplitudes are close to the true values. Moreover, the standard deviation of the main frequency amplitude is small while this value is relatively large for first engine order amplitude. However by looking at the histogram given in Figure 4.15, it is seen that around 80% of the amplitude values are accumulated in the interval $[0.5, 1]$ that is still an acceptable performance considering the true value which is equal to 0.8682. The conclusion is that by fixing the $C_{\text{eng,load}}$ to some value in the interval $[1, 10]$, which may not be true, the performance loss can be assumed negligible. In other words, two important properties of the damping wheel angular velocity, i.e. the amplitudes of engine first order and the main frequency, will not change significantly in the simulated output.

Table 4.10: *Statistical properties of the engine* 1*st order and the main frequency amplitudes obtained by Monte Carlo simulation in which the damping coefficient* $C_{eng,load}$ *is varying uniformly in the interval* $[1, 10]$*, Operating point* $<$ 1200 *RPM,*$\sim$ 57 *N.m*$>$*.*

Statistics / Amplitude	Min	Max	Mean	STD	True
1st engine order (RPM)	0.4963	2.3709	0.8222	0.3818	0.8682
Main frequency (RPM)	5.9916	6.3757	6.2323	0.1108	6.92

Model performance for the other engine operating points

The final discussion of this section is devoted to the influence of altering the engine operating point on the estimated model behavior. So far the applied operating point was similar for both the estimation and validation data sets, i.e. $<$ 1200 RPM,$\sim$ 57 N.m$>$. But it is interesting to study whether the predicted angular velocity can follow the measured signal at the other engine speeds and loads. Figure 4.16 shows the simulated response from the estimated grey-box model $\mathfrak{m}_{\text{eng},r}$ at different operating points than the one which has been used during estimation. As it is seen, the predicted angular velocities cannot anymore follow the actual signal trend and that is due to wrong friction coefficient C_{eng}. According to the given description in Section 3.1.1 of Chapter 3, the engine friction depends on different properties including engine operating point, namely speed and load. Therefore, the estimated value for $C_{\text{eng}} = 0.1541$ at $<$ 1200 RPM,$\sim$ 57 N.m$>$ is not valid when either of speed or load is changed. A map of the friction coefficient value for the simplified 2 DOF model of Figure 4.2 at different engine speeds and loads is given in Table 4.11. This is obtained by estimating of C_{eng} while the other model parameters, i.e. $\frac{1}{J_{\text{eng}}}$, $C_{\text{eng,load}}$, $K_{\text{eng,load}}$, and $\frac{1}{J_{\text{load}}}$ are fixed. Using the values given in Table 4.11, it is possible to interpolate for the desired operating point. It is seen that the friction coefficient decreases by increasing the speed whereas at higher loads the friction is also bigger.

Figure 4.17 depicts the predicted angular velocity versus measured signal at operating point $<$ 1400 RPM,$\sim$ 67 N.m$>$ in which $C_{\text{eng}} = 0.1421$ according to Table 4.11. As it is seen, by correcting the friction coefficient, the model can follow the trend of measured angular velocity more accurately in comparison to the plots given in Figure 4.16.

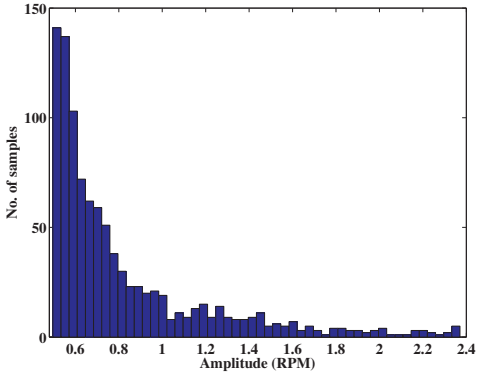

(a) *1st engine order amplitude.*

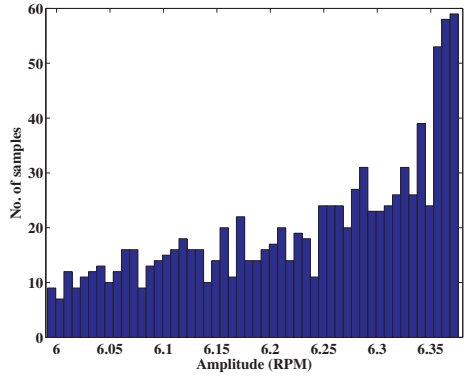

(b) *Main engine frequency amplitude.*

Figure 4.15: *Histograms of the engine* 1*st order and the main frequency amplitudes for* 1000 *times simulation in which the damping coefficient* $C_{eng,load}$ *is varying uniformly in the interval* $[1, 10]$*, Operating point* $<$ 1200 *RPM,*$\sim$ 57 *N.m*$>$*.*

4.3 Parameter estimation of the 7 DOF model

In this section, the unknown parameters of the 7 DOF engine-load lumped structure, shown in Figure 3.6 and represented with the LTI state-space model (3.13), are estimated. Similar to 2 DOF simplified model identification, the 7 DOF estimated model will be validated against a fresh data set by evaluating the model fit as well as performing residual analysis.

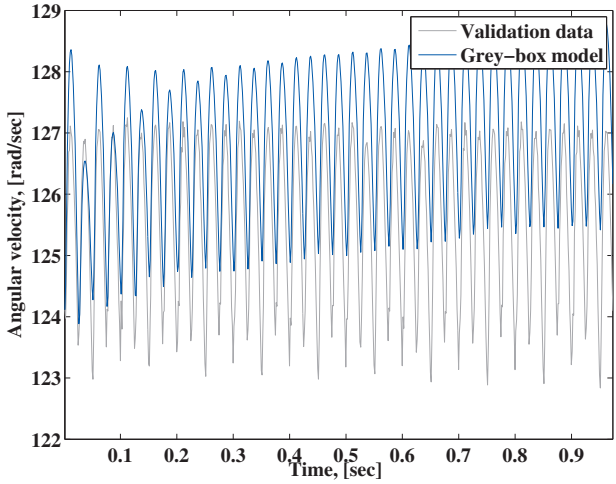

(a) $< 1200\ RPM, \sim 67\ N.m >$.

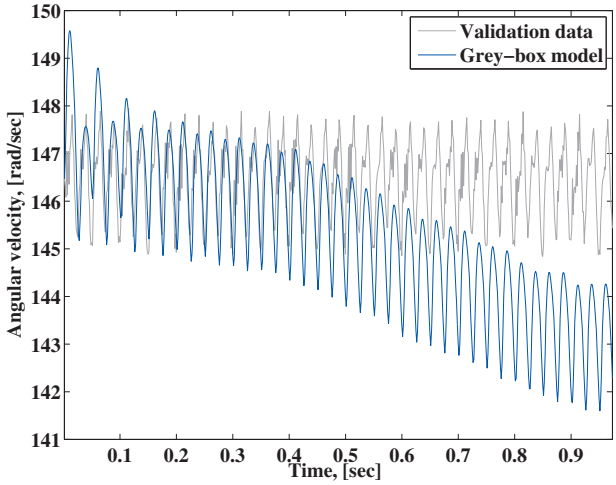

(b) $< 1400\ RPM, \sim 57\ N.m >$.

Figure 4.16: *Examples of model response by changing engine load or speed, true output signal (gray) and simulated output (blue) from the grey-box model* $\mathfrak{m}_{eng,r}$ *which has been estimated at operating point* $< 1200\ RPM, \sim 57\ N.m >$.

Table 4.11: *Estimated values of friction coefficient C_{eng} for different engine speeds (RPM) and loads (N.m).*

Speed \ Load	50	60	70	80	90	100
1000	0.1895	0.1959	0.2042	0.2116	0.2188	0.2319
1200	0.1541	0.1621	0.1707	0.1771	0.1826	0.1907
1400	0.1354	0.1421	0.1504	0.1558	0.1565	0.1628
1600	0.1182	0.1240	0.1286	0.1355	0.1399	0.1412
1800	0.1134	0.1136	0.1189	0.1246	0.1261	0.1337
2000	0.1007	0.1054	0.1116	0.1172	0.1172	0.1225

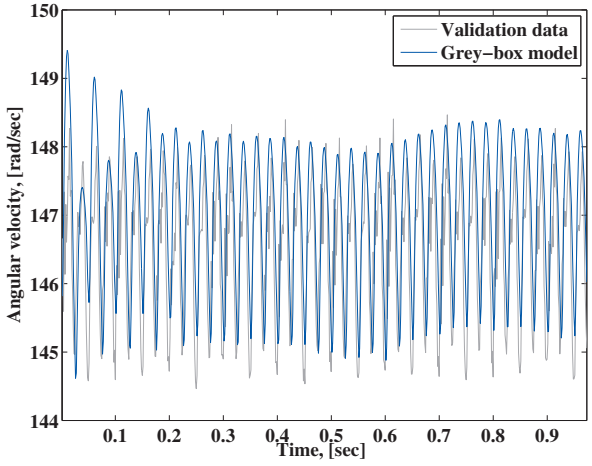

Figure 4.17: *Model response (blue) versus true output signal (gray) at new operating point* <1400 *RPM,*~ 67 *N.m*$>$ *using* $C_{eng} = 0.1421$ *while the other model parameters are the same as in Table 4.7.*

4.3.1 Problem statement

The LTI state-space model structure $\mathbb{M}_{\text{eng},7}$ for the 7 DOF engine-load system is again given here:

$$\begin{aligned} \dot{x}(t) =& A(p)x(t) + B(p)u(t) \\ z(t) =& \dot{\theta}_1(t) = [1\ 0...0]x(t) \end{aligned} \tag{4.12}$$

where, as described in Section 3.3.1, the state vector is as follows

$$\begin{aligned} x_{13\times 1} =& \big[\dot{\theta}_1, \dot{\theta}_2, \theta_2 - \theta_1, \dot{\theta}_3, \theta_3 - \theta_2, \dot{\theta}_4, \theta_4 - \theta_3 \\ & \dot{\theta}_5, \theta_5 - \theta_4, \dot{\theta}_6, \theta_6 - \theta_5, \dot{\theta}_7, \theta_7 - \theta_6\big]. \end{aligned} \tag{4.13}$$

The input vector of (4.12) is

$$u(t) = [T_{\text{tot},1}(t),\ T_{\text{tot},2}(t),\ T_{\text{tot},3}(t),\ T_{\text{tot},4}(t),\ T_{\text{load}}(t)]^{\text{T}} \tag{4.14}$$

in which by using the linear assumption described in Sections 3.3.1 and 4.2.1, the input vector can be calculated separately. The system matrices $A(p)$ and $B(p)$ are given in Appendix A. The known characteristics of the engine are given in Table 4.2. The vector of unknown parameters $p_{\text{eng},7}$ for the engine-load model structure $\mathbb{M}_{\text{eng},7}$ includes both the model physical parameters and the unknown feedback terms $K(p)$. The number of physical parameters in (4.12) is in total 23, i.e. stiffness, damping, and inertia coefficients. However J_7 and K_{76} have been obtained previously in Section 4.2.2 and are given in Table 4.7. Thus, 21 parameters remain to be estimated. This is too many for the PEM which has a limitation in the number of unknown parameters for the current model structure and available data due to occurrence of different local optima in the optimization algorithm. The first solution to this problem is to assume the same structure for each crank-slider mechanism in Figure 3.6. Therefore

$$\begin{gathered} J_2 = J_3 = J_4 = J_5, \\ K_{32} = K_{43} = K_{54},\ \ C_{32} = C_{43} = C_{54},\ \ C_2 = C_3 = C_4 = C_5 \end{gathered} \tag{4.15}$$

which results in decreasing the number of unknowns to 11. To decrease this number further, the total engine friction C_{eng}, that has been found already for 2 DOF model, is also applied for the current structure. Hence, by using the assumptions given in (4.15),

$$C_2 = C_3 = C_4 = C_5 = \frac{C_{\text{eng}}}{4}. \tag{4.16}$$

Finally, according to the discussion in Section 4.2.1, estimation of damping coefficient at the same time with the other model parameters has a destructive effect on the identification performance. Therefore C_{21}, C_{32}, C_{65}, and C_{76} in Figure 3.6 are fixed to the known values which are found from literature, see for example Rabeih (1997); Ponti (2008). These values can be further revised by evaluating the amplitudes of the engine orders as mentioned in Section 4.2.2. So, the 6 parameters which are to be estimated are: J_1, J_2, J_6, K_{21}, K_{32}, and K_{65}. As discussed for the simplified 2 DOF model, before starting any estimation procedure, the structural identifiability of these 6 unknown parameters should be studied. Here the Mathematica package `IdentifiabilityAnalysis`, as mentioned in Section 2.2.2, is used to perform the rank test on the extended observability matrix, since the 7 DOF model is rather large with 13 states and 6 unknown parameters. The maximum rank is found equal to 19 which indicates that all the 6 parameters are identifiable assuming informative input. The Mathematica code is attached in Appendix A.

4.3.2 Results

The collected measurements at operating point <1200 RPM,~ 57 N.m$>$ are again used for identification here which include 10 engine working cycles, totally 14400 samples with sampling frequency ~ 14402 Hz. In this section, the first 6 engine cycles of normal combustions are applied as estimation data while further the estimated 7 DOF model is validated against the remaining 4 engine cycles. Figure 4.18 shows the measured input and output data set for the model structure $\mathbb{M}_{\text{eng},7}$ given in (4.12). As described in (4.14), the input vector has 5 elements while the output is damping wheel angular velocity.

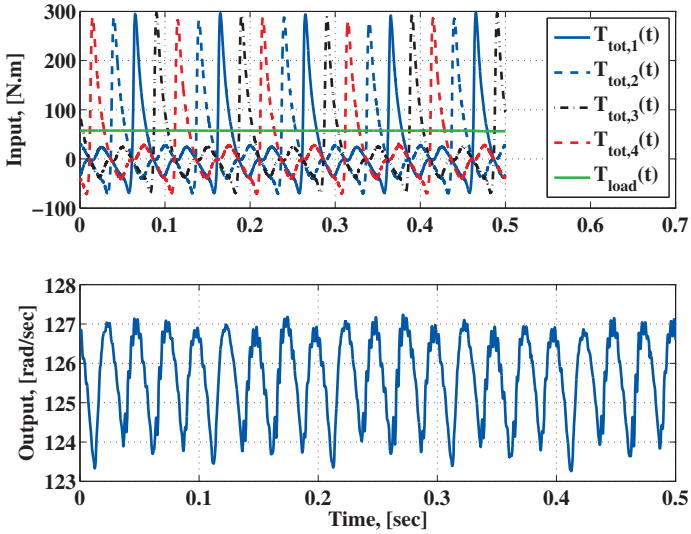

Figure 4.18: *Example of measured input and output data used for identification of 7 DOF model structure $\mathbb{M}_{eng,7}$, Operating point <1200 RPM,~ 57 N.m$>$. Five engine cycles has been plotted here.*

Table 4.12 presents the estimation results of the 7 DOF model structure $\mathbb{M}_{\text{eng},7}$. It contains the fit percentage to validation data, the estimated parameter values, and their corresponding estimated covariances. Due to the reasons mentioned before concerning the linearity, the inverse of J_1, J_2 and J_6 are estimated. Moreover, as described in Section 4.2.2, to increase the identification performance and model quality the measurements should be down-sampled with different factors until the correlations decrease to an acceptable level. Here, down-sample factor 15 is sufficient. The relatively high estimation covariances in Table 4.12, in comparison to the results given in Table 4.7, is a result of greater number of unknown parameters in the 7 DOF model structure.

The validation procedure starts with comparing the estimation results given in Table 4.12 with the four-cylinder SI engine parameters provided by Ponti (2008). The estimated inertia coefficients agree well with the values given in this

Table 4.12: *Estimated parameters for continuous-time 7 DOF model structure $\mathbb{M}_{eng,7}$ given in (4.12). Estimation data is resampled normal combustion input/output at operating point < 1200 RPM,∼ 57 N.m> with sampling frequency ∼ 14402/15 = 960.1 Hz.*

	Estimated	Covariance
$\frac{1}{J_1}$	33.39	7
$\frac{1}{J_2}$	22.3	0.2
$\frac{1}{J_6}$	5.968	0.02
K_{21}	241.8 E03	728
K_{32}	1270 E03	771
K_{65}	1427 E03	1209
fit(%)	43.21	

paper while the determined stiffness coefficients are also in the same range as the results presented in Ponti (2008). The residual analysis which is performed on a fresh data set is the second step of validation which is used here to study the reliability of current model structure and estimation approach. This can be claimed if there exist low correlations between the residuals themselves as well as low cross-correlations of the residuals and inputs. Figure 4.19 gives the results of the residual analysis which show that the correlations are approximately within 99% confidence interval.

4.3.3 Comparison of 2 DOF and 7 DOF models using mode shape analysis

As described previously, the actual engine-load system first resonance occurs at 20 Hz, see Table 4.6. However, since the engine measurements are available up to 2000 RPM for the current thesis, it was not possible to find the other resonance frequencies of the system. Furthermore, it has been indicated that the 2 DOF model structure also has a natural frequency at 20.34 Hz. In this section, an eigenvalue evaluation is performed for the 7 DOF model to obtain its natural frequencies as well as the corresponding modal shapes. This helps determine the deformation between different inertias at each resonance frequency and thus define how much the model can be further simplified depending on the frequency region of interest.

Table 4.13 gives the natural frequencies and the associated deformation difference between two consecutive inertias for the 7 DOF model structure $\mathbb{M}_{\text{eng},7}$. The model is given in (4.12) with the estimated parameters in Table 4.12. For the state vector definition, see (4.13). As can be seen, for the system first mode 20.5 Hz there is no specific deformation in the crankshaft part and the major deformation happens at the connection between the engine and the load, $\theta_7 - \theta_6$. Indeed, the main crankshaft deformation begins at the second mode, i.e. 335 Hz.

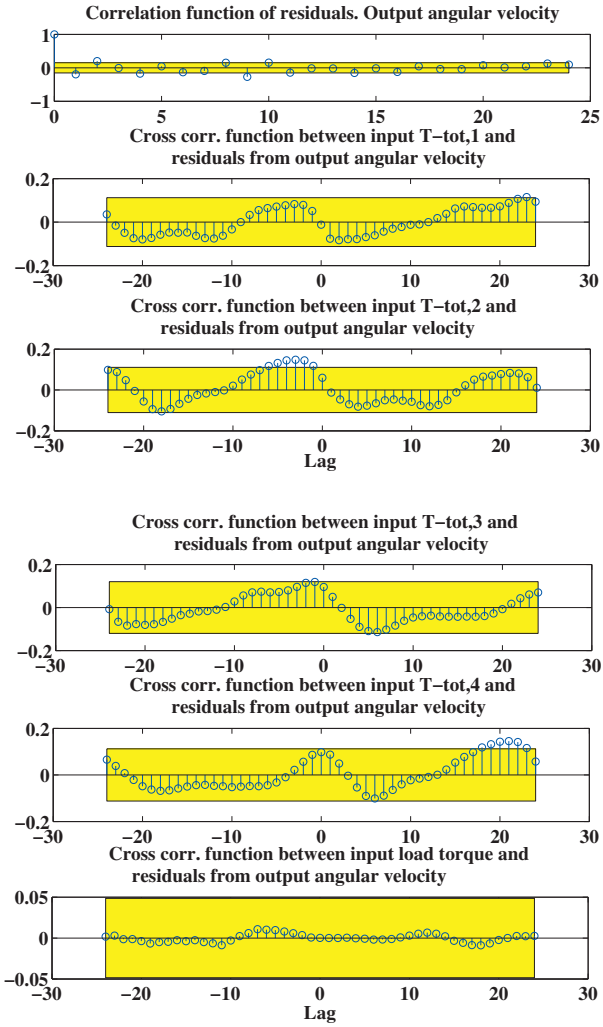

Figure 4.19: *Residual analysis of* 7 *DOF model structure* $\mathbb{M}_{eng,7}$ *given in (4.12) using the resampled validation data set with sampling frequency* $\sim 14402/15 = 960.1$ *Hz.*

Therefore, it can be concluded that for the applications in which the frequency region of interest is lower than 300 Hz, it is sufficient to consider the crankshaft as a rigid body. Thus, the simplified 2 DOF model structure $\mathbb{M}_{\text{eng}}$ given in (4.9) can be applied in these cases. This is a very important result from the aspect of the identification procedure. It has been shown earlier in this thesis how much the PEM algorithm is sensitive to the number of unknown parameters for the current model structure and available data. Moreover, most of the analysis such

as identifiability are less complicated when it comes to the smaller systems.

Table 4.13: *The natural frequenies (N. Freq.) in Hz and the associated normalized modal shapes (M. Shape) for the 7 DOF model structure* $\mathbb{M}_{eng,7}$*. The absolute values of deformations are shown.*

N. Freq. \ M. Shape	$\theta_2-\theta_1$	$\theta_3-\theta_2$	$\theta_4-\theta_3$	$\theta_5-\theta_4$	$\theta_6-\theta_5$	$\theta_7-\theta_6$
20.5	0.0007	0.0003	0.0005	0.0007	0.0008	1
335	1	0.3229	0.4038	0.4216	0.3322	0.6414
548	1	0.0692	0.1030	0.2109	0.2085	0.1501
936	1	0.7600	0.7693	0.1636	0.7937	0.1953
1340	0.4898	1	0.4202	0.7870	0.7273	0.0873
1604	0.2091	0.6531	1	0.9355	0.4324	0.0363

Besides the natural frequencies given in Table 4.13, there is a zero natural frequency which, as described in Section 4.2.2, is called rigid body mode. At this mode the angular deformations between all the inertias remain constant.

Figure 4.20 depicts the 7 DOF model simulated output $\hat{y}_s(t|\mathfrak{m}_{\text{eng},7})$ versus the measured validation data. As it is seen, the higher frequency content in the true signal, which is greater than 300 Hz, can be almost captured by the 7 DOF model which was not the case for the 2 DOF model. The amplitudes of the higher frequencies can be corrected by modifying the damping coefficients or trying to estimate these values applying different kinds of measurements and estimation methods than those used here. This is beyond the scope of this thesis and considered as a future work.

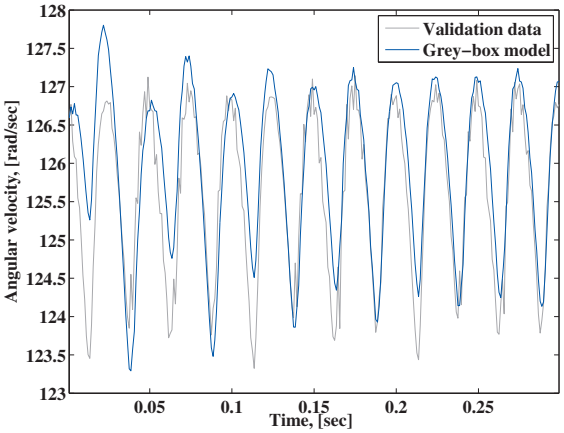

Figure 4.20: *True output signal (gray) and simulated output (blue) from the estimated 7 DOF grey-box model* $\mathfrak{m}_{eng,7}$ *for measured validation data, sampling frequency* $\sim 14402/15 = 960.1$ *Hz.*

Chapter 5

Applications

In the previous chapters, a mathematical model for reproducing torsional behavior of an engine-load system has been developed in which a four-cylinder four-stroke internal combustion spark ignited engine has been considered. Two different versions of this model, i.e. 2 DOF and 7 DOF structures, have been identified to achieve a good agreement between the modeled and the measured damping wheel angular velocities as the system output. The frequency region of interest implies which version of the model is appropriate for the current application. Having the estimated model ready, two main applications of this type of modeling for engine/driveline torsional vibrations are given in a brief format in this chapter. The first application considers the ride quality evaluation which is based on the results of Nickmehr et al. (2012). Misfire detection is the second case which is introduced here and is still an ongoing project.

5.1 Ride quality evaluation of a passenger car

The powertrain system is an assembly of active and reactive elements which is highly nonlinear and lightly damped and can be easily excited by external sources such as road inputs. It can itself be a source of Noise, Vibration, and Harshness (NVH) where different kinds of vibrations are possible in a wide frequency range $2 - 5000$ Hz. An example of a passenger car powertrain vibration spectrum for linear torsional cases is given in Table 5.1, see Farshidianfar et al. (2002).

Table 5.1: *An Example of a passenger car powertrain vibration spectrum.*

Freq. Range (Hz)	Exciting Force	Phenomenon
$2-8$ (Vibration)	Engine torque variation *E.g., sudden throttle application*	Surge/ Shuffle (Longitudinal)
$20-50$ (Vibration- Boom noise)	Engine torque variation	Wind-up
$50-80$ (Boom noise)	Engine torque variation *E.g., engine torque fluctuation*	Drive train torsional vibration

The ride interval includes the frequencies between $1-100$ Hz. This frequency range has been reported by ISO for evaluation of passenger comfort to the whole body vibrations, see Wong (2008). A passenger car is ready for sale when the seat vibrations, at the traveling speed of 80 km/h on a typical inter-urban road, is approximately close to the ISO limitations, see Harrison (2004). As mentioned by Nickmehr et al. (2012), ride dynamic system investigation contains three main parts. First, introduction of major excitation sources, such as engine/driveline and road irregularities. Second, determining vehicle dynamic response subject to these excitations and, third, the human perspicacity. In Nickmehr et al. (2012), a powertrain torsional vibration model has been presented which is composed of different subsystems, i.e. crankshaft of four-cylinder four-stroke IC engine, transmission, differential, drive shaft, and wheels. The model parameters were the typical values from literature and no estimation was performed. It has been explained that the engine vibrations, which are due to the delivered engine fluctuating torque, are transferred to the chassis through suspension system. This produces a longitudinal vibration in low frequency which might decrease the passenger comfort. Moreover, a linear 2 DOF suspension system, known as the quarter-car model, was used to obtain vertical acceleration of the vehicle-body due to the road disturbing input. The results are shown here in Figure 5.1 in which the Root Mean Square (RMS) acceleration of the model in longitudinal and vertical directions have been obtained. Moreover, these plots are compared to the ISO fatigue-decreased proficiency boundaries during a four-hour exposure time in vertical and longitudinal directions. It is assumed that the vehicle is traveling with a constant speed of 80 km/h on an average road roughness. As can be seen, the vehicle-body vertical response subject to the road irregularities is greater than the objective criteria at the frequency region around $1-11$ Hz using the suspension system given in Nickmehr et al. (2012). However the longitudinal acceleration, resulting from the transferred engine torque excitations, is under the ISO boundary. For detail information about the model and its parametrization see Nickmehr et al. (2012).

Based on this discussion, it is crucial to have a suitable crankshaft model which can accurately predict the system response to the engine torque for further applying of this model as a subsystem of an entire powertrain system. The modeling and identification approach in this thesis not only provides this desired model for the crankshaft system, it also proposes a methodology which is usable

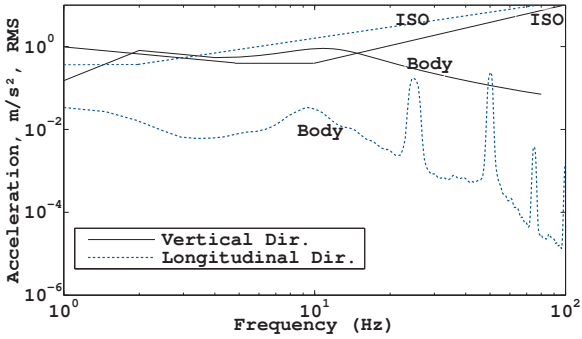

Figure 5.1: *Comparison of body RMS accelerations in different directions with ISO criteria.*

to estimate the unknown parameters in the other powertrain subsystems. This can be achieved using the same modular structure as presented here and having more available measurements in different parts of powertrain such as transmission or wheels.

5.2 Misfire modeling

In Chapter 2, it was shown that the misfire data set is useful to identify the unknown parameters of the developed model structure $\mathbb{M}_{\text{eng}}$, given in (4.9) and Figure 4.2, where these parameters could not be found using normal combustion data. The reason is the important effects of misfire on the damping wheel angular velocity in the actual engine-load setup and therefore on the J_{eng} angular velocity that is representing the entire crankshaft in the simplified 2 DOF model. This is known as crankshaft wind-up and carries new information which is helpful for parameter estimation as well as misfire detection. However, when other disturbances such as cold start, auxiliary load variations, road load excitations, or even another misfire happen simultaneously, their corresponding oscillations on the damping wheel angular velocity interact with each other, destructively. Thus, it is not an easy task to distinguish between their effects on the angular velocity and the associated test quantity. Therefore, in this section the estimated model is applied to investigate how different kinds of input excitations can complicate misfire detection. By performing a qualitative validation of the model, it can be concluded that the predicted angular velocity from the model captures the amplitude and oscillatory behavior of the actual data as well as the influences of misfire. This plus the simulation results from injecting the other disturbances to the 2 DOF identified engine-load torsional vibration model, are beneficial to evaluate and optimize misfire detection algorithms.

Figure 5.2 depicts the estimated 2 DOF model response for 10 engine working

cycles when there is no misfire as well as in a situation where a misfire occurs in cylinder 2 at time ~ 0.35 s. The results show a relatively good agreement between the model and the measurements in terms of frequency and amplitude of oscillation. Therefore in misfire modeling, the simplified model structure is sufficient. The explanation for the deviation between measurement and simulation in the misfire case, mainly in the mean value of the angular velocity, may come from inaccuracy in the experiment. This is probable, especially for the pressure and torque measurements which affect the system input. Performing these experiments at a wide range of engine speed and load will help understand the system behavior better. Consequently more accurate model identification can be done. This is an ongoing project and considered as a future work.

Figure 5.3 shows the FFT of the measured angular velocity signal for normal and misfire data sets. As it is seen when misfire is present, the signal frequency content is different which is significant in the frequency range below 50 Hz. This is also a good clarification for using the 2 DOF model in the misfire modeling. In other words, as mentioned in Section 4.3.3, the simplified model structure is appropriate enough for the frequency range below 300 Hz which is the interval we are interested in for the misfire application. These generated vibrations may cause a problem in detection of a second misfire happening close to the first one, see Ponti (2008). Having a suitable model can help modify the misfire detection algorithm to compensate for undesired vibrations due to multiple misfires or other possible disturbances.

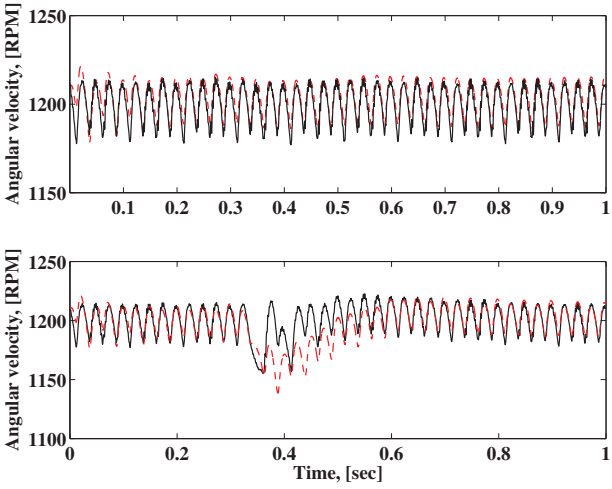

Figure 5.2: *Experimental (solid) and simulated (dashed) angular velocities at operating point* $<$ 1200 *RPM,*$\sim$ 57 *N.m*$>$*. Above: Normal combustion data set, Below: Misfire data set.*

Auxiliary load variations, such as turning on and off the air condition, can be considered as an additional torque applied on the damping wheel of the engine-

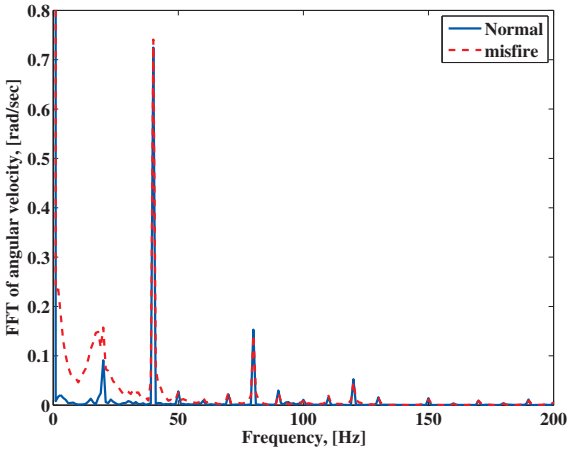

Figure 5.3: *Frequency content of measured angular velocity signal for two cases of normal and misfire data set at operating point* $<$ 1200 *RPM,*$\sim$ 57 *N.m*$>$.

load setup, see Eriksson et al. (2013). Therefore to inject a change in auxiliary load, in the simplified 2 DOF model, a negative step torque can be added to the $T_{\text{tot,eng}}(t)$ which is one of the system input, see (4.9) and (4.4). There is no measured angular velocity for this excitation and hence in Figure 5.4 only the simulation results from the estimated 2 DOF model are presented. The measured in-cylinder pressures at operating point $<$ 1200 RPM,$\sim$ 57 N.m$>$ have been used to calculate the engine torque. The second disturbance which is interesting to model here is a sudden excitation in the road load which can be entered to the system by imposing an impulse on the required torque $T_{\text{load}}(t)$. Figure 5.4 gives also the simulation results of this road excitation. As it is illustrated, the estimated 2 DOF model response, i.e. angular velocity of J_{eng}, subject to these two mentioned disturbances is approximately similar to the results in Figure 5.2 which shows the misfire case. Therefore, if any auxiliary load variation or road torque disturbances occur at the same time with misfire, may interfere in the misfire detection algorithm. Accordingly, acquiring an appropriate and not complicated simulation model for engine torsional vibrations beforehand is a useful tool for robustness analysis of detection algorithms.

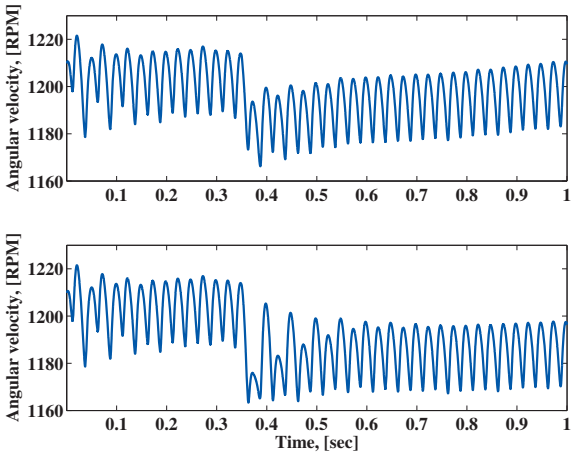

Figure 5.4: *Simulated angular velocity at* < 1200 *RPM,*~ 57 *N.m*$>$*. Above: Auxiliary load change, Below: Sudden excitation in road torque.*

Chapter 6

Conclusions and future work

The goal of this thesis is to propose and evaluate a modeling and identification approach for engine-load system torsional vibration description. The applications of interest are ride quality investigation for passenger cars as well as modifications in misfire detection algorithms using model-based analysis. In the thesis, a four-cylinder four-stroke internal combustion spark ignited engine has been considered and two main steps have been performed to achieve the goal.

The first step treated developing a mathematical model for describing the engine-load system torsional vibrations. To do this, only the torsional behavior of the crankshaft system has been modeled while the other possible types of vibrations, such as bending and axial, were not taken into account. The proposed model is modular and thus it can be conveniently reconfigured for example to model an engine with different number of cylinders. It has been shown that the actual distributed system can be presented by a 7 DOF lumped spring-mass-damper structure in which the viscous damping law has been applied to model the engine friction. Further, the total fluctuating engine torque has been calculated as the system input which is also the main source of excitation in an engine-load setup. The step one was completed by giving the linear time invariant state-space formulation of the model structure. It is composed of some unknown physical parameters which have been estimated in step two using grey-box modeling and PEM as the estimation technique.

The step two started with simplifying the 7 DOF model structure to a 2 DOF version which the simulation study has been performed on. The outcomes of estimation on simulation data indicated two essential points which helped further modify the estimation performance, see Section 4.2.1. The first point was about the convergence property of damping coefficients. It was shown that fixing these parameters improves the estimation accuracy for the current model structure and available data set. The second point considers the data information importance for identification precision. It has been concluded that by using a

normal combustion data set, the estimated parameters do not match the true values, however this problem has been solved when the misfire data set was applied. Step two continued with performing estimation on real data using both 2 DOF and 7 DOF model structures. Grey-box modeling plus the PEM, which were explained in Chapter 2, have been used for model identification. Further, the identified models have been validated against a fresh data set in which the low correlations in residual analysis implied the model quality. However, the correlations were high when the original sampling frequency was considered and it was presented that down-sampling of the original measurements results in a better model behavior and the correlations stay almost inside the 99% confidence interval. Moreover, the simulated angular velocity follows the measured signal even in operating points different from that of the estimation data set. As a final validation, it was shown that the estimated models could capture the actual system's first natural frequency around 20 Hz. Step two finished with modal shape analysis of the 7 DOF system in Section 4.3.3 to prove that the 2 DOF model structure is sufficient for the frequency range below 300 Hz. If the application of interest concerns the higher frequencies, then the 7 DOF model structure is suggested. Even though, as it was shown in Section 4.3, the results of the simplified model estimation can still be used in the larger model identification to decrease the number of unknowns and consequently improve the estimation variances.

In Chapter 5, misfire as well as two other disturbances, i.e. auxiliary load variation and road load excitation, have been injected to the simplified 2 DOF model structure. For the misfire case, it has been shown that measurement and simulation agree with each other in terms of frequency and amplitude. Moreover, it has been indicated that the generated torsional vibrations due to the misfire occurrence resemble the influences of the two other disturbances. This can introduce a problem in the misfire detection algorithm. Therefore, a reliable model has two important benefits. First, it can help study and optimize the detection algorithms robustness subject to the effects of the other possible external disturbances. Second, a simulation model prevents doing expensive experimental investigations for developing a misfire detection algorithm since the initial studies are useful to analyze the actual system.

The future studies of this work contain three main issues. First, the parameters of the in-cylinder pressure model, which is given in Eriksson and Andersson (2002), are to be identified using a wide range of engine measurements in different speeds and loads. In a real car operation, the pressure measurements are not available and if the model is intended to be used in detection at real time, an appropriate pressure model is also essential, see Eriksson et al. (2013). Second, a suitable identification technique is to be presented for estimating damping coefficients. As it was shown, the PEM and the current measurements could not be used for estimating these parameters in a reliable way. Third, it is to be studied how the rest of powertrain system can be modeled and identified which is applicable in the passenger car ride quality evaluation.

References

M. Anguelova. *Observability and identifiability of nonlinear systems with applications in biology*. PhD thesis, Chalmers University of Technology, 2007.

F.T. Connolly and G. Rizzoni. Real time estimation of engine torque for the detection of engine misfires. *Journal of Dynamic Systems, Measurement, and Control*, 116(4):675–686, 1994.

Ph. Couderc, J. Callenaere, J. Der Hagopian, G. Ferraris, A. Kassai, Y. Borjesson, L. Verdillon, and S. Gaimard. Vehicle driveline dynamic behaviour: experimentation and simulation. *Journal of sound and vibration*, 218(1):133–157, 1998.

A. Crowther. Powertrain vibration: Modeling, simulation and testing. In *FISITA World Automotive Congress*, Barcelona, Spain, 2004.

D. Dowson. *History of Tribology, 2nd Edition*. Wiley, 1998.

D. Eriksson, L. Eriksson, E. Frisk, and M. Krysander. Flywheel angular velocity model for misfire and driveline disturbance simulation. In *7th IFAC Symposium on Advances in Automotive Control*, Tokyo, Japan, 2013.

L. Eriksson and I. Andersson. An analytic model for cylinder pressure in a four stroke SI engine. In *SAE Technical Paper 2002-01-0371*, 2002. doi:10.4271/2002-01-0371.

L. Eriksson and L. Nielsen. *Modeling and control of engines and drivelines*. Wiley, 2014.

A. Farshidianfar, M. Ebrahimi, H. Bartlett, and M. Moavenian. Driveline shuffle in rear wheel vehicles. *International Journal of Heavy Vehicle Systems*, 9(1):76–91, 2002.

Z.S. Filipi and D.N. Assanis. A nonlinear, transient, single-cylinder diesel engine simulation for predictions of instantaneous engine speed and torque. *Journal of engineering for gas turbines and power*, 123(4):951–959, 2001.

T. Glad and L. Ljung. *Control Theory*. CRC Press, 2000.

F. Gustafsson, L. Ljung, and M. Millnert. *Signal Processing*. Studentlitteratur, 2010.

M. Harrison. *Vehicle Refinement, Controlling Noise and Vibration in Road Vehicles*. SAE International, 2004.

R. Hermann and A.J Krener. Nonlinear controllability and observability. *IEEE Transactions on automatic control*, 22(5):728–740, 1977.

R. Johansson. Modeling of engine and driveline related disturbances on the wheel speed in passenger cars. Master's thesis, Linköping University, 2012.

R.E. Kalman. A new approach to linear filtering and prediction problems. *Journal of Fluids Engineering*, 82(1):35–45, 1960.

J. Karlsson, M. Anguelova, and M. Jirstrand. An efficient method for structural identiability analysis of large dynamic systems. In *16th IFAC Symposium on System Identification*, Brussels, Belgium, 2012.

U. Kiencke. Engine misfire detection. *Control Engineering Practice*, 7(2): 203–208, 1999.

Dr. D. Kopeliovich. Bearings in internal combustion engines. `http://www.substech.com/dokuwiki/lib/exe/fetch.php?w=&h=&cache=cache&media=internal_combustion_engine.png`, 2014. Accessed: 2014-09-25.

L. Larsson, Z. Sjanic, M. Enqvist, and L. Ljung. Direct prediction-error identification of unstable nonlinear systems applied to flight test data. In *15th IFAC Symposium on System Identification*, Saint-Malo, France, 2009.

O. Leufven. Engine laboratory. `http://www.fs.isy.liu.se/Lab/EngineLab/`, 2013. Accessed: 2014-09-25.

J. Linder, M. Enqvist, F. Gustafsson, and J. Sjöberg. Identifiability of physical parameters in systems with limited sensors. In *Proceedings of the 19th IFAC World Congress*, Cape Town, South Africa, 2014.

C.Q. Liu and R.L. Huston. *Principles of Vibration Analysis, With Applications in Automotive Engineering*. SAE International, 2011.

L. Ljung. *System Identification Toolbox User's Guide*. The MathWorks, Inc., 1988-2014.

L. Ljung. *System Identification: Theory for the User*. Prentice Hall, 1999.

L. Ljung. Perspectives on system identification. *Annual Reviews in Control*, 34 (1):1–12, 2010.

L. Ljung and T. Glad. On global identifiability for arbitrary model parametrizations. *Automatica*, 30(2):265–276, 1994.

L. Meirovitch. *Fundamentals of Vibrations*. Waveland Pr Inc., 2010.

J. Mohammadpour, M. Franchek, and K. Grigoriadis. A survey on diagnostic methods for automotive engines. *International Journal of Engine Research*, 13 (1):41–64, 2012.

N. Nickmehr, J. Åslund, L. Nielsen, and K. Lundahl. On experimental-analytical evaluation of passenger car ride quality subject to engine and road disturbances. In *The 19th International Congress on Sound and Vibration (ICSV19)*, Vilnius, Lithuania, 2012.

R. Nicolas. Introduction to internal combustion engine. `http://www.car-engineer.com/fr/files/2012/12/Featured-image-ICE.png`, 2012. Accessed: 2014-09-25.

F. Ollivier. Inversibility of rational mappings and structural identifiability in automatics. In *Proceedings of the ACM-SIGSAM 1989 international symposium on symbolic and algebraic computation*, pages 43–54, 1989.

F. Ponti. Development of a torsional behavior powertrain model for multiple misfire detection. *Journal of Engineering for Gas Turbines and Power*, 130(2), 2008.

E. Rabeih. *Torsional Vibration Analysis of Automotive Driveline*. PhD thesis, The university of Leeds, 1997.

H. Rahnejat. *Multi-Body Dynamics: Vehicle, Machines, and Mechanisms*. Wiley, 2005.

D. Ranjan. Slider crank mechanism (i.c. engine). Captured from `http://www.youtube.com/watch?v=HkyjMItf-1Y`, 2011. Accessed: 2014-09-25.

P.D. Richardson. Free oscillations with damping proportional to the square of the velocity. *Applied Scientific Research, Section A*, 11(4-6):397–400, 1963.

G. Rizzoni and Y. Zhang. Identification of a non-linear internal combustion engine model for on-line indicated torque estimation. *Mechanical Systems and Signal Processing*, 8(3):275–287, 1994.

D. Sandoval and J. B. Heywood. An improved friction model for spark-ignition engines. In *SAE Technical Paper 2003-01-0725*, 2003. doi:10.4271/2003-01-0725.

S. Schagerberg and T. McKelvey. Instantaneous crankshaft torque measurements - modeling and validation. In *SAE Technical Paper 2003-01-0713*, 2003. doi:110.4271/2003-01-0713.

A. Sedoglavic. A probabilistic algorithm to test local algebraic observability in polynomial time. *Journal of Symbolic Computation*, 33:735–755, 2002.

T. Söderström and P. Stoica. *System Identification (Prentice Hall International Series in Systems and Control Engineering)*. Prentice Hall, 1988.

P. Soltic. *Part-Load Optimized SI Engine Systems, Appendix E: Engine Friction Models*. PhD thesis, Swiss Federal Institute Of Technology Zürich, 2000.

F.V. Tinaut, A. Melgar, H. Laget, and J.I. Domnguez. Misfire and compression fault detection through the energy model. *Mechanical Systems and Signal Processing*, 21(3):1521–1535, 2007.

E. Walter. *Identifiability of State Space Models: With Applications to Transformation Systems*. Lecture Notes in Biomathematics. Springer-Verlag Berlin, 1982.

J.Y. Wong. *Theory of Ground Vehicles*. Wiley, 2008.

Appendix A

7 DOF system matrices and Mathematica code

System matrices for the 7 DOF system which has been shown in Figure 3.6 and represented with the LTI state-space model (3.13).

$$B(p) = \begin{bmatrix} 0 & 0 & 0 & 0 & 0 \\ \frac{1}{J_1} & 0 & 0 & 0 & 0 \\ 0 & 0 & 0 & 0 & 0 \\ 0 & \frac{1}{J_2} & 0 & 0 & 0 \\ 0 & 0 & 0 & 0 & 0 \\ 0 & 0 & \frac{1}{J_3} & 0 & 0 \\ 0 & 0 & 0 & 0 & 0 \\ 0 & 0 & 0 & \frac{1}{J_4} & 0 \\ 0 & 0 & 0 & 0 & 0 \\ 0 & 0 & 0 & 0 & 0 \\ 0 & 0 & 0 & 0 & 0 \\ 0 & 0 & 0 & 0 & -\frac{1}{J_7} \\ 0 & 0 & 0 & 0 & 0 \end{bmatrix} \tag{A.1}$$

$A(p) =$

Columns 1:4

$$\begin{array}{cccc}
-\frac{1}{J_1}C_{21} & \frac{1}{J_1}C_{21} & \frac{1}{J_1}K_{21} & 0 \\
\frac{1}{J_2}C_{21} & -\frac{1}{J_2}(C_{21}+C_{32}+C_1) & -\frac{1}{J_2}K_{21} & \frac{1}{J_2}C_{32} \\
-1 & 1 & 0 & 0 \\
0 & \frac{1}{J_3}C_{32} & 0 & -\frac{1}{J_3}(C_{32}+C_{43}+C_2) \\
0 & -1 & 0 & 1 \\
0 & 0 & 0 & \frac{1}{J_4}C_{43} \\
0 & 0 & 0 & -1 \\
\vdots & \vdots & \vdots & \vdots \\
0 & 0 & 0 & 0
\end{array}$$

Columns 5:8

$$\begin{array}{cccc}
0 & 0 & 0 & 0 \\
\frac{1}{J_2}K_{32} & 0 & 0 & 0 \\
0 & 0 & 0 & 0 \\
-\frac{1}{J_3}K_{32} & \frac{1}{J_3}C_{43} & \frac{1}{J_3}K_{43} & 0 \\
0 & 0 & 0 & 0 \\
0 & -\frac{1}{J_4}(C_{43}+C_{54}+C_3) & -\frac{1}{J_4}K_{43} & \frac{1}{J_4}C_{54} \\
0 & 1 & 0 & 0 \\
0 & \frac{1}{J_5}C_{54} & 0 & -\frac{1}{J_5}(C_{54}+C_{65}+C_4) \\
0 & -1 & 0 & 1 \\
0 & 0 & 0 & \frac{1}{J_6}C_{65} \\
0 & 0 & 0 & -1 \\
0 & 0 & 0 & 0 \\
0 & 0 & 0 & 0
\end{array}$$

Columns 9:13

$$\begin{array}{ccccc}
0 & 0 & 0 & 0 & 0 \\
\vdots & \vdots & \vdots & \vdots & \vdots \\
0 & 0 & 0 & 0 & 0 \\
\frac{1}{J_4}K_{54} & 0 & 0 & 0 & 0 \\
0 & 0 & 0 & 0 & 0 \\
-\frac{1}{J_5}K_{54} & \frac{1}{J_5}C_{65} & \frac{1}{J_5}K_{65} & 0 & 0 \\
0 & 0 & 0 & 0 & 0 \\
0 & -\frac{1}{J_6}(C_{65}+C_{76}) & -\frac{1}{J_6}K_{65} & \frac{1}{J_6}C_{76} & \frac{1}{J_6}K_{76} \\
0 & 1 & 0 & 0 & 0 \\
0 & \frac{1}{J_7}C_{76} & 0 & -\frac{1}{J_6}C_{76} & -\frac{1}{J_7}K_{76} \\
0 & -1 & 0 & 1 & 0
\end{array} \tag{A.2}$$

The mathematica code for structural identifiability analysis of the 7 DOF model with 13 states and 6 unknown parameters

In[868]:=
```
Needs["IdentifiabilityAnalysis`"];
```

In[869]:=
```
deq = {
    x1'[t] == alpha * (K21 * x3[t] + 15 * (-x1[t] + x2[t])), x1[0] == meas,
    x2'[t] == beta * (-K21 * x3[t] - 15 * (-x1[t] + x2[t]) + K32 * x5[t] +
         2.5 * (-x2[t] + x4[t]) + input1[t] - (0.1541 / 4) * x2[t]), x2[0] == meas,
    x3'[t] == (-x1[t] + x2[t]), x3[0] == 0,
    x4'[t] == beta * (-K32 * x5[t] - 2.5 * (-x2[t] + x4[t]) + K32 * x7[t] +
         2.5 * (-x4[t] + x6[t]) + input2[t] - (0.1541 / 4) * x4[t]), x4[0] == meas,
    x5'[t] == (-x2[t] + x4[t]), x5[0] == 0,
    x6'[t] == beta * (-K32 * x7[t] - 2.5 * (-x4[t] + x6[t]) + K32 * x9[t] +
         2.5 * (-x6[t] + x8[t]) + input3[t] - (0.1541 / 4) * x6[t]), x6[0] == meas,
    x7'[t] == (-x4[t] + x6[t]), x7[0] == 0,
    x8'[t] == beta * (-K32 * x9[t] - 2.5 * (-x6[t] + x8[t]) + K65 * x11[t] +
         2.5 * (-x8[t] + x10[t]) + input4[t] - (0.1541 / 4) * x8[t]), x8[0] == meas,
    x9'[t] == (-x6[t] + x8[t]), x9[0] == 0,
    x10'[t] == gamma * (-K65 * x11[t] - 2.5 * (-x8[t] + x10[t]) +
         1992 * x13[t] + 2.5 * (-x10[t] + x12[t])), x10[0] == meas,
    x11'[t] == (-x8[t] + x10[t]), x11[0] == 0,
    x12'[t] == 5.646 * (-1992 * x13[t] - 2.5 * (-x10[t] + x12[t]) - input5[t]),
    x12[0] == meas,
    x13'[t] == (-x10[t] + x12[t]), x13[0] == 0};

measured = {x1[t]};
iad = IdentifiabilityAnalysis[{deq, measured},
  {x1, x2, x3, x4, x5, x6, x7, x8, x9, x10, x11, x12, x13},
  {alpha, beta, gamma, K21, K32, K65, meas},
  t, {input1, input2, input3, input4, input5}]
iad["IdentifiableQ"]
```

Out[871]=
```
IdentifiabilityAnalysisData[True, <>]
```

Out[872]=
```
True
```